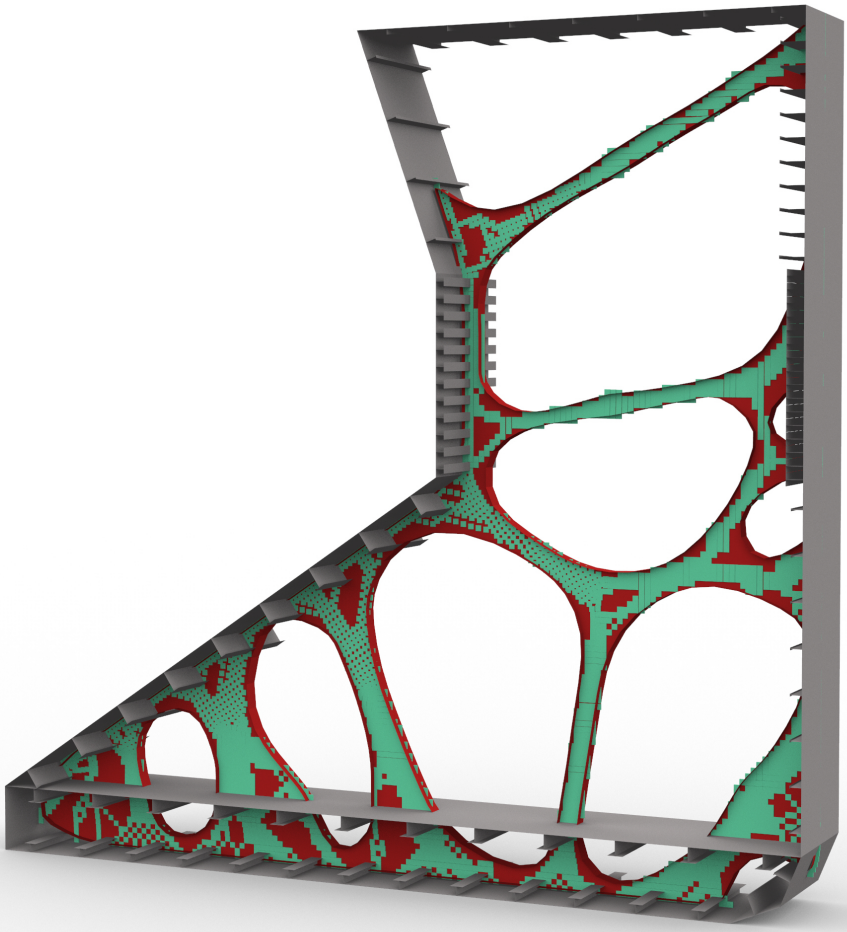

Shape and Topology Optimized TSHD Midsection

H.W. Vuijk

Technische Universiteit Delft

TU Delft

Shape and Topology Optimized TSHD Midsection

by

H.W. Vuijk

Student number: 4230922
Project duration: May 20, 2019 – April 14, 2020
Thesis committee:

Prof. ir. J.J. Hopman,	TU Delft
Dr. ir. J.H. den Besten,	TU Delft
Ir. M.P.G.J. Verdult,	Vuyk Engineering Rotterdam
Dr. ir. M. Langelaar,	TU Delft
Dr. C.L. Walters,	TU Delft

TU Delft VUYK

Summary

The common practice of designing a ship is to look for ships with similar specifications and alter it to the client's needs. This often leads to structurally redundant and therefore overdimensioned ship designs. Hence, much improvement could be expected from ship structures where optimization algorithms help advise in the design process. In this research, the midsection of a Trailing Suction Hopper Dredger (TSHD) is optimized. A TSHD midsection generally consists of longitudinal stiffened panels and transverse web frames. The typical web frame and longitudinal stiffener layout is optimized, as a weight improvement of this section can have a large effect on the total weight of the ship since it is repeatedly reoccurring.

This research has optimized the midsection of a reference TSHD in two ways; the first step was to perform a shape optimization for the longitudinal stiffener arrangement, which was followed by a topology optimization for the transverse web frame. Both optimization objectives were to minimize mass. The order of optimization follows the hierarchy in which stresses are introduced into the structure; from the plates that make up the hull toward the stiffeners and eventually the web frames. The complete optimization was performed a total of seven times, for seven different web frame spacings ranging from 25% to 175% of the web frame spacing of the reference TSHD.

For the shape optimization, a Simulated Annealing algorithm was used. The reference ship was simplified to be able to parameterize the geometry into eleven panels with T-stiffeners. Each panel has a set of variables that describe its geometry; the plate thickness, number of stiffeners, stiffener web height, flange width and web and flange thicknesses. Although feasible results came out of the optimization, no clear parallel was found when comparing the plates of different web frame spacings. This is due to the fact that it is a high dimensional problem. Although no clear parallels were found, the results were able to cope with all the loads.

The topology optimization was performed with a modified Bi-directional Evolutionary Structural Optimization (MBESO) method. The applied modifications ensure a fast convergence for large topology optimization problems. The new method was first verified by comparing results to two benchmark cases from the original BESO method, which was followed by three examples of common topology optimization benchmarks. Once established that the modified method was capable of reproducing test cases, an aspect ratio analysis was performed to better understand the transmission of stress. After that, the full geometry of the midsection was divided into smaller basic models and the same optimization was carried out in order to help interpret underlying physics of the final results. Finally, the topology optimizations for the seven web frame spacings were performed, resulting in a new orientation of beams. The topology optimization results showed that constructing beams not in an orthogonal way and along the ship hull but rather under various angles could reduce the total mass of the web frame.

To see how the shape optimization result influenced the topology optimization, three studies were carried out where all the surrounding plates had the same thickness, except for one that would have a significant smaller thickness. This showed how the web frame supports the hull plating, but also how the web frame is dependent on the stiffness of certain panels to be able to transfer shear into them.

Finally a comparison was made between the reference ship and the optimized structure. The result was a decrease of 23% in weight for the midsection. Due to practical production considerations this weight is likely to be higher in practice, however it is a promising start toward a more efficient ship design. The innovative combination of shape optimization combined with the MBESO procedure could help in early design stages where the main components of the construction are defined.

Acknowledgements

This thesis completes the Master of Science programme at Delft University of Technology. The research was carried out at Vuyk Engineering Rotterdam.

Doing this research has been an incredible and educational experience. From the start I mentioned that the topic provided by Vuyk and the TU would have been similar to what I would describe as the perfect research problem to dedicate my graduation thesis to.

I would like to thank Henk den Besten for his catching enthusiasm and astounding amount of experience in ship structures and interest of implementing optimization. I would also like to thank Michiel Verdult for all of his time spent on meetings, providing an ample amount of feedback on the report and guiding the research with his tremendous amount of experience in ship design. On top of that I would also like to thank Matthijs Langelaar to help me in a crucial time to better understand and implement the topology optimization. Next to that I would also like to thank Carey Walters and Hans Hopman to take part in the thesis comittee.

I would also like to express my gratitude toward my parents who have helped me keep a positive mindset during the research. Furthermore, I would like thank Floortje in motivating and supporting me in every way possible. Finally I would like to thank my friends with whom I live with helping me unwind after a hard day's work.

I hope you enjoy reading the report!

Contents

I Topic Analysis **1**

1 Introduction **3**
1.1 Context . . . 3
1.2 Problem Statement . . . 3
1.3 Significance . . . 4

2 Literature Review **5**
2.1 Buckling Analysis . . . 5
2.1.1 Euler Buckling Theory . . . 5
2.2 Shape Optimization . . . 7
2.2.1 Principles . . . 7
2.2.2 Simulated Annealing . . . 8
2.3 Topology Optimization . . . 9
2.3.1 History . . . 9
2.3.2 Approaches . . . 9
2.3.3 Comparison . . . 11
2.3.4 Conclusion . . . 12
2.4 Shape and Topology Optimization in Ship Structures . . . 12

3 Research Objectives **15**
3.1 Research Questions . . . 15
3.2 Research Subquestions . . . 15
3.3 Methodology . . . 15

II Models and Results **17**

4 Stiffened Panel Model **19**
4.1 Introduction . . . 19
4.2 Geometry . . . 19
4.3 Loading . . . 20
4.4 Geometry Variables . . . 20
4.5 Analytical Model . . . 21
4.5.1 Moment of Inertia . . . 21
4.5.2 Yield . . . 23
4.5.3 Linear Buckling . . . 23
4.5.4 Constraints . . . 25
4.5.5 Simulated Annealing . . . 25
4.5.6 Optimization Procedure . . . 26
4.6 Numerical Analysis of Analytical Solutions . . . 26
4.7 Results . . . 26
4.8 Discussion . . . 27
4.8.1 Constraint Influence . . . 27
4.8.2 Differences Analytical and Numerical Results . . . 28
4.8.3 Trends in Stiffened Panels . . . 28
4.8.4 Numerical Procedure . . . 29

5 Web Frame Model **31**
5.1 Introduction . . . 31
5.2 Modified BESO . . . 31
5.2.1 Neighbour Inclusion Ratio . . . 31
5.2.2 Random Start . . . 31
5.2.3 Absence of Volume Constraint . . . 32
5.2.4 Ratios . . . 32
5.2.5 Optimization Procedure . . . 33
5.2.6 Verification of MBESO . . . 33
5.3 Geometry . . . 39
5.4 Loading . . . 39
5.5 Optimization Parameter Setting . . . 40
5.6 Web Frame Thickness . . . 40
5.7 Underlying Mechanisms . . . 41
5.7.1 Aspect Ratio Analysis . . . 41
5.7.2 Reduced Models . . . 42
5.8 Results . . . 43
5.9 Discussion . . . 44
5.9.1 Common Beams . . . 44
5.9.2 Neighbour Inclusion Ratio with Random Start . . . 46
5.9.3 Deflection . . . 46
5.9.4 Random Start . . . 47
5.9.5 Limitation . . . 47
5.9.6 MBESO Coarseness . . . 47
5.9.7 Design Tool . . . 47

6 Optimization Interaction **49**
6.1 Introduction . . . 49
6.2 Results . . . 49
6.3 Discussion . . . 49

7 Optimal Web Frame Spacing **51**
7.1 Midsection Comparison . . . 51
7.2 Abstraction Procedure . . . 52
7.3 Discussion . . . 53

III Conclusions and Recommendations **55**

8 Conclusion **57**

9 Recommendations **59**

IV Appendix and Bibliography **61**

A Direct Numerical Optimization Results **63**
A.1 Simulated Annealing . . . 63
A.2 Result . . . 64
A.3 Discussion . . . 64

B Appropriate Web Frame Thickness Analysis **65**

C Supplementary Fundamental Model Results **67**

D Supplementary Web Frame Topology Optimization Results **69**

Bibliography **73**

List of Symbols and Abbreviations

σ_Y	Yield stress
$\sigma_{VM,e}$	Von Mises stress in element
b_e	effective width
B_p	plate breadth
BESO	Bi-directional Evolutionary Structural Optimization
BV	Bureau Veritas
c_x	centroid along x-axis
c_z	centroid along z-axis
E	Young's Modulus
$E_e[i,k]$	Young's Modulus of element k in iteration i
e_s	element size
ESO	Evolutionary Structural Optimization
F(x)	Fitness of x
FEA	Finite Element Analysis
FEA(x)	Finite Element Analysis of model with variable vector x
FEM	Finite Element Method
FIS	Fully Included Start
H	Hopper pressure due to sludge
h_w	web height
I_x	moment of inertia around x-axis
IR	Inclusion Ratio
L	Length
MBESO	Modified Bi-directional Evolutionary Structural Optimization
n_e	number of elements
n_s	number of stiffeners
NIR	Neighbour Inclusion Ratio
ON	Oscillation Number
PSA	Plate-Stiffener Analytical
PSN	Plate-Stiffener Numerical
RR	Rejection Ratio

RS	Random Start
SA	Simulated Annealing
SO	Shape Optimization
SOV	Sets of Variables
ss	Stiffener Spacing
t_f	flange thickness
t_p	plate thickness
t_w	web thickness
TO	Topology Optimization
TSHD	Trailing Suction Hopper Dredger
W	Water pressure
w_f	width of flange
WFS	Web Frame Spacing

I

Topic Analysis

1 Introduction

1.1. Context

Large ships are mainly constructed of longitudinal stiffened panels combined with web frames and bulkheads. It is a good combination that can withstand loads induced by the sea and cargo. This way of constructing a ship has been the conventional method and has proven to be a redundant design. However, a shipyard and designer would always prefer to use the least amount of material possible to reduce cost and weight, which in turn can increase the payload. To achieve that, finite element analysis (FEA) has been combined with optimization techniques to find the most ideal layout of stiffeners and shape of the web frame. However, most of these methods do not include a buckling analysis in the iterations. That would mean that these mechanisms have to be studied after the first layout has been determined and may result in changing the design. To overcome this, the full static strength check should be incorporated into the optimization.

Topology optimization (TO) and shape optimization (SO) can both be used to reduce the mass. The difference between the two are the variables that are presented to the algorithm to alter. With TO, several methods can be used to find the optimum geometry but in this research each meshed element has its own E modulus ranging from zero to the E modulus of steel. This approach allows for organic structures. The SO uses the stiffener parameters as its variables. Examples of these are the web height and thickness, flange height and thickness and stiffener spacing.

1.2. Problem Statement

The design space of this problem is the midsection of a Trailing Suction Hopper Dredger (TSHD), consisting of a web frame and stiffened panels. The outer hull and hopper geometry of the structure are predefined and will not change during the optimization. The longitudinal stiffened panels will be subject to the SO since the stiffener arrangement can be parameterized. The transverse web frame to the TO to give the opportunity to find a new orientation of transverse beams.

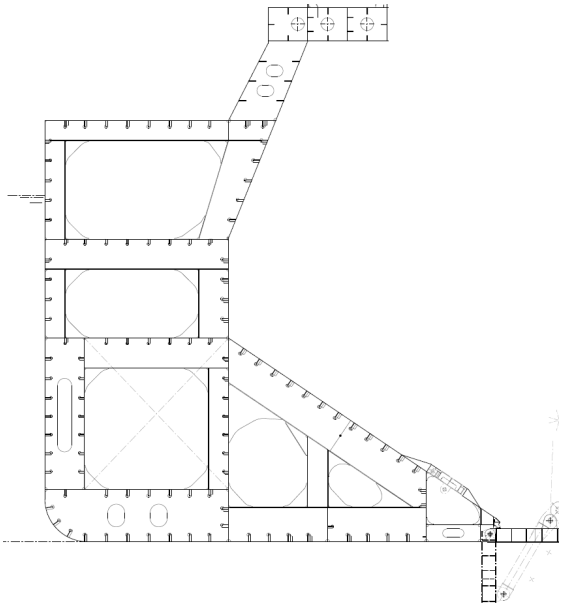

Figure 1.1: Typical midsection of TSHD (courtesy of Vuyk Engineering)

1.3. Significance

Industry's interest
The fact that all ships now are designed with more structural redundancy than accounted for is not necessarily a bad situation. However, it is always helpful to know how the structure can be improved. The results of the shapes can be unprofitable to build, but it will show the dependencies of structural members and the direction a feasible design could take to improve on minimizing mass.

This research is now focused on the midsection of a hopper dredger, but will eventually be easily transformed to be applicable to all kind of ship types.

Research interest
There is a gap in today's knowledge about designing in early stages toward fatigue and buckling simultaneously. This holistic approach would improve the structure or reduce post processing time with FEA. Moreover, the combination of TO and SO on this scale has not yet been applied.

On top of that, the design question will be turned around. At the moment the most conventional way of designing a ship structure is to look back on previous designs that are similar and configuring that to a structure that satisfies all the design requirements. This new way of starting the design loop begins by asking 'what does the structure want to look like?'.

Stakeholder's interest
For Vuyk Engineering designing dredgers has become one of their specialties. Over time, a considerable amount of hopper dredger designs have been delivered and the search for the optimum design is desired. However, when the tool is working it should be easy to change the hull shape to any midsection of any other ship possible.

2
Literature Review

Before going into the models, an overview of all the pertinent theory must be described. This chapter reviews most of the used literature and acts as a toolbox with theory that will be applied in the models.

2.1. Buckling Analysis

To assess the buckling load, three main approaches can be used. Firstly the non-linear approach which will have an accurate result of the buckling load, but it is a rather computational expensive method. Another one is the eigenvalue analysis, which is linear and less accurate but a lot faster to calculate. This method assumes a perfect structure without any defects and that is one of the reasons why it always over-estimates the actual critical load as can be seen in Figure 2.1. A third option is to use a rule based system. This is the most conservative, but realistic way of assessing the structure as it accounts for defects and is also altered over the years to incorporate more redundancy where required through experience. The most important factor for this research tool is the calculation speed as it will be used in an iterative procedure. This cancels out the non-linear buckling analysis.

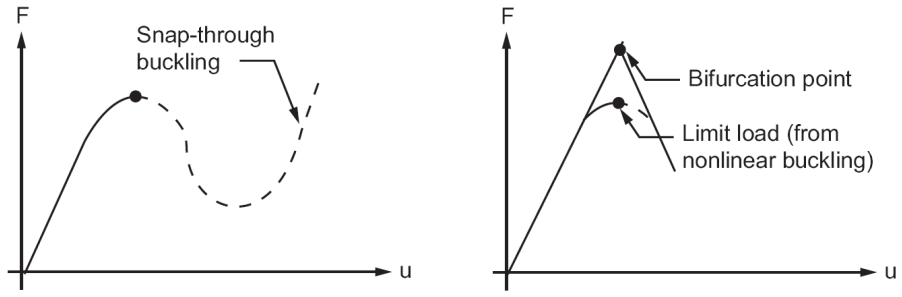

Figure 2.1: F is compressive force and u the deflection. (left) non-linear buckling analysis. (right) linear buckling analysis [2]

2.1.1. Euler Buckling Theory

Euler buckling is a linear analysis and can be easily adopted into a large amount of iterations as the time it consumes to calculate is relatively short. One of the main dependencies of buckling is the slenderness of the structure. The equations below describe the slenderness ratio of a column: [17]

$$\lambda = l/k = l/\sqrt{I/A} \tag{2.1}$$

Where l is the effective length of a column and k is the radius of gyration. This states that a long and flexible column is more prone to buckle under a lower critical stress by:

$$\sigma_{cr} = \pi^2 E \frac{I}{A}\frac{1}{l^2} = \pi^2 E \left(\frac{l}{k}\right)^2 \tag{2.2}$$

That is the critical buckling load, also referred to as the Euler buckling stress, for a column that is simply supported at both ends as this yields a larger l than a clamped beam and therefore a conservative approach.

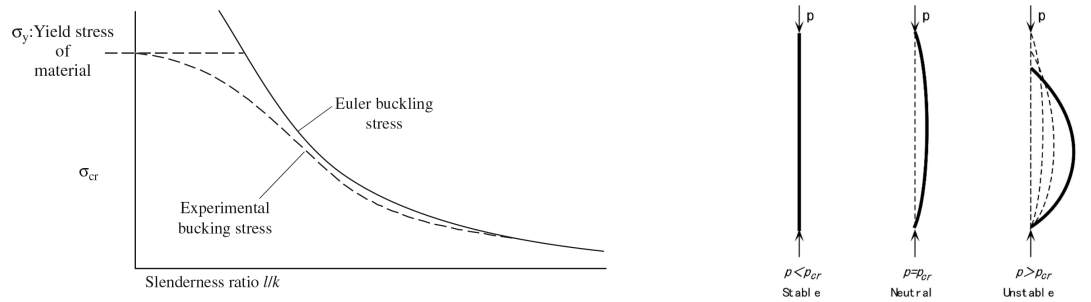

Figure 2.2: (a) Euler buckling curve. (b) Column buckling under compressive stress.[17]

From Figure 2.2a it is evident that when the slenderness becomes small, the buckling load will be extremely large. That is however bound by the yield stress of the material. To approach the experimental buckling stress, a few alternatives have been made:

$$\begin{aligned} \sigma_{cr} &= a - b(\frac{l}{k}) \quad \textit{Tetmayers's formula} \\ \sigma_{cr} &= a - b(\frac{l}{k})^2 \quad \textit{Johnson's formula} \\ \sigma_{cr} &= \frac{a}{1 + b(l/k)^2)} \quad \textit{Rankine's formula} \end{aligned} \tag{2.3}$$

Where a and b make up the cut-trough dimensions of the column.

The same principles apply to the buckling of plates but now a and b represent the width and length of the plate and therefore $\alpha = a/b$.

When assumed that the plate is simply supported around the edges it is a conservative approach, just as with the column. The shape that this plate will have when buckling is described by the following formula [17]:

$$w = f \cdot sin(\frac{m\pi x}{a}) \cdot sin(\frac{n\pi y}{b}) \tag{2.4}$$

Considering that the elastic buckling stress is a minimum critical stress [17]:

$$\sigma_e = \frac{\pi^2 E}{12(1-\nu)^2} \cdot (\frac{t}{b})^2 \cdot K \cdot \eta \quad with \quad K = min((\frac{m}{\alpha} + \frac{\alpha}{m})^2) \tag{2.5}$$

$$where \quad \eta = \begin{cases} 1 & \sigma_e \leq \sigma_Y/2 \\ \frac{\sigma_Y}{\sigma_e} - \frac{1}{4}(\frac{\sigma_Y}{\sigma_e})^2 & \sigma_e > \sigma_Y/2 \end{cases} \tag{2.6}$$

The factor η is used for the same reason the Euler buckling curve is altered in Equations 2.3. When the factor b/t becomes too small, the σ_{cr} will be higher than the yield stress. η is the Johnson's modification factor.

A stiffened panel is most likely exposed to more stresses than only the compression over one side. A more elaborate visualization is shown in Figure 2.3b where the in plane stress varies over one of the sides, creating a moment. On top of that a lateral pressure is imposed on the structure, resembling water pressure on a hull. All these buckling influences will be the base for the analytical approach formulated in in Section 4.5.3.

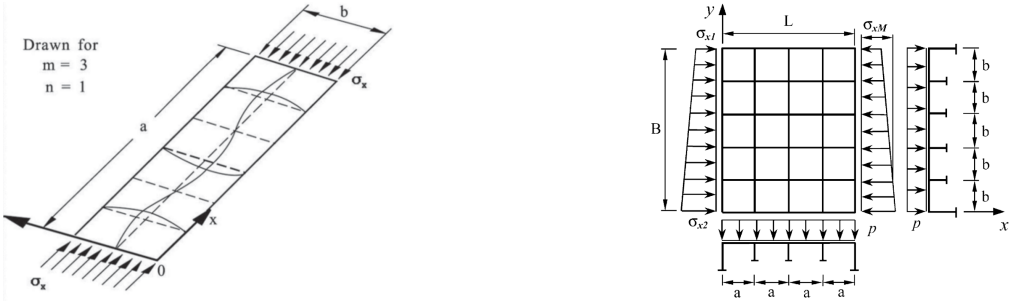

(a) (b)

Figure 2.3: (a) Plate buckling under compressive stress with modeshape of 3 half waves in x direction and 1 half wave in y.[18] (b) Plate under combined longitudinal axial stress, longitudinal in-plane bending and lateral pressure.[19]

2.2. Shape Optimization

2.2.1. Principles

The structure is parameterized into a handful of variables which define the full geometry. Examples of these variables are thickness of a material, width of a truss or radius and location of a void. Whether the variables are continuous or discrete is dominant in the selection for the optimization algorithm.[13]

The optimization algorithm will be used in the SO. This is a discrete problem due to the fact that 'number of stiffeners' will be a variable and that must be an integer. Global optimization methods can handle discrete variables whereas gradient based methods are only applicable to continuous problems.

The standard problem formulation for optimization methods is the following:

$$\begin{aligned} f_i(x) &= min \quad y(x) \\ g_i(x) &\leq 0 \\ h_i(x) &= 0 \end{aligned}$$

Where f resembles an objective function, g stands for an inequality constraint which are mostly converted to be less than or equal to 0. The same is done for the set of equality constraints h_i. The complete problem is dependent on the set of variables x.

Figure 2.4 shows a 2 dimensional continuous objective function as an example where $d = 2$, $m = 5$, the matrix a and vector c [14]:

$$\text{a} = \begin{bmatrix} 3 & 5 \\ 5 & 2 \\ 2 & 1 \\ 1 & 4 \\ 7 & 9 \end{bmatrix} \quad \text{and c} = \begin{bmatrix} 1 \\ 2 \\ 5 \\ 2 \\ 3 \end{bmatrix}$$

$$f(x_1, x_2): \quad min \quad -\sum_{i=1}^{m} c_i \cdot exp\left(-\frac{1}{\pi}\sum_{j=1}^{d}(x_j - a_{ij})^2\right) cos\left(\pi \sum_{j=1}^{d}(x_j - a_{ij})^2\right)$$

$$\begin{aligned} g_1(x_1, x_2): &\quad -x_1, -x_2 \leq 0 \\ g_2(x_1, x_2): &\quad (x_1 - 10), (x_2 - 10) \leq 0 \\ h(x_1, x_2): &\quad not \quad applied \end{aligned}$$

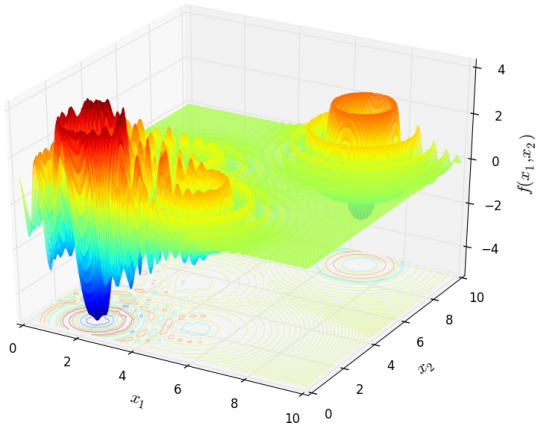

Figure 2.4: Example 2D Langermann optimization problem. [9]

It shows a local minimum around $f(7,9)$ and the global optimum at approximately $f(2,1)$. When it is stated that some algorithms can get trapped in a local minima, it means that the optimization gets stuck at point $f(7,9)$ and is unable to escape and work toward $f(2,1)$. This figure also demonstrates the difficulties in visualizing a higher dimensional optimization problem, as with these plots the maximum amount of variables is 2.

2.2.2. Simulated Annealing

The shape optimization problem that will be adopted is a discrete optimization problem because the amount of stiffeners is discrete. On top of that, for one iteration it will only use one function evaluation as opposed to for instance a genetic algorithm which requires the amount of function evaluations equal to the population size. This makes the SA computationally more attractive. The basis of this algorithm is the 'greedy hill climber'. That optimization method only accepts a set of variables that results in a higher fitness for the next iteration. The problem with that method is that it might get stuck in a local optimum because it cannot escape out of the valley (when minimizing). Another part of the basis is the 'random search' algorithm. The name is self-explanatory, which means that it makes random sets of variables without comparing them during the iterations and hoping to find a good solution.

The combination of the two is the 'simulated annealing' (SA) [8]. It will always accept a better solution, but in the beginning of the optimization process it is also likely that the current solution will be overridden by a worse set of variables. This combines both of best worlds; a greedy hill climber with a random search to be able to escape local minima.

The optimization loop toward an optimum is shown below:

$$
\begin{aligned}
C &= x_{random} \\
&for \quad T \quad in \quad range(T_{max}, \quad T_{min}, \quad n_{iterations}) \\
&\quad F_{current} = F(C) \\
&\quad N = x_{random} \\
&\quad F_{new} = F(N) \\
&\quad \Delta F = F_{current} - F_{new} \\
&\quad if \quad (\Delta F > 0) \\
&\quad\quad C = N \\
&\quad elseif \quad (e^{\frac{\Delta F}{T}} > random(0,1)) \\
&\quad\quad C = N \\
&\quad else \\
&\quad\quad C = C \\
&\quad endif \\
&endfor
\end{aligned}
$$

Since the T vector starts at its maximum value and gradually works to it minimum, the $e^{\frac{\Delta F}{T}} > random(0,1)$ criterion becomes more strict toward the end of the optimization. If the ΔF is negative, it means that the new value for F is higher and thus a worse solution. However, it will result in a $e^{\frac{\Delta F}{T}}$ between 0 and 1, with a $\frac{\Delta F}{T}$ of larger magnitude closer to 0. That means that if the ΔF is small and T still large, it is more likely to be larger than $random(0,1)$ and therefore accepting it as the solution for the next iteration. This also implies that when T is small, it will produce a large negative $e^{\frac{\Delta F}{T}}$ and resulting in a value closer to 0, therefore less likely to pass the $e^{\frac{\Delta F}{T}} > random(0,1)$ criterion. This is why in the beginning of the optimization, worse solutions can be accepted for the next iteration, but approaching the final iterations it is far less likely to do so.

2.3. Topology Optimization

2.3.1. History

With topology optimization the goal is to find the best distribution of material in a given design domain [4]. One of the earliest adaptations to this philosophy has been synthesized by A.G.M. Michell [12, 16] who analytically approached an optimal arrangement of bars to form a frame. However, this approach but was found to be not practical and therefore only stayed in the academic realm. Around half a century later the work was continued and led to different topology optimization approaches including; the homogenization method SIMP by Bendsoe [11], level set by Allaire [1], phase field by Boudrin and Chambolle [3] and evolutionary approaches by Xie and Steven [25].

2.3.2. Approaches

Various approaches include the fitness function to be a minimization of compliance (maximization of stiffness), maximum performance or a minimization of mass. The applied constraints vary from a maximum allowable stress or deflection and minimum volume. Although a range of different approaches exist, this research will mainly focus on element based optimization which include 'evolutionary' and its close relative 'density based' Solid Isotropic Material with Penalization (SIMP). This choice was made as the element approach is a relatively easy comprehensible and implementable approach.

SIMP Method

The Solid Isotropic Material with Penalization method created by Bendsoe and Kikuchi in 1988 [11] has the objective to minimize strain energy density per element $W_{den,e}$.

$$W_{den,e} = \frac{\frac{1}{2}u_e^T K_e u_e}{V_e} \tag{2.7}$$

The density of an element is linked to its stiffness E_e, therefore reducing the density will also reduce its stiffness. When the fitness function is derivated by the density the following sensitivity is created:

$$E_e = \rho_e^p \cdot E_{0,e} \quad , \qquad K_e = \rho_e^p \cdot K_{0,e} \tag{2.8}$$

Where the change in the elemental Young's Modulus E_e is the same as the change in its elemental stiffness K_e. When K_e is implemented in Equation and derived over the density ρ_e, the following sensitivity equation is realised:

$$\frac{\delta W_{den,e}}{\delta \rho_e} = -p \cdot \rho_e^{p-1} \frac{\frac{1}{2}u_e^T K_{0,e} u_e}{V_e} \tag{2.9}$$

Every element has its own fitness function and therefore also its own sensitivity analysis. The goal is to minimize the strain energy density by altering the stiffness of the element which is done with the Young's modulus. This is a convex function within the the range with ρ_e between 0 and 1. This density variable is not picked from a linear line between 0 and 1, but rather ρ_e^p. That way the algorithm is forced to pick values closer to 0 and 1, as this tends to yield better results in terms of less moderately filled elements. This virtual density and therefore stiffness are what is called the homogenization method. It resembles an element of the structure that is partially filled and is partially a void, but is homogenized to have the same amount of stiffness and density.

To find the density for the element in the next iteration, the sensitivity is set to zero.

$$\frac{\delta W_{den,e}}{\delta \rho_e} = 0 \tag{2.10}$$

Because this is a continuous function it can be solved with a gradient based optimization algorithm. After creating the geometry and initializing the optimization, each iteration consists of the steps depicted below.

1. calculate strain energy densities for each element
2. find ρ_e where sensitivity equals 0
3. set this value for next iteration

This continues until the stopping criteria have been met. Examples of these are volume constraints or maximum amount of iterations.

Evolutionary

This is a discrete type of optimization where the elements can be either an idle or included element as opposed to the SIMP method where can be anything between a minimal value and 1. The original version of ESO and BESO is in fact an unconstrained optimization type and focuses on the stress. As there is no constraint on either the minimal amount of volume or maximum stress. The final result can only be influenced by tuning the parameters and this takes some experience. While during the optimization no constraints are used, it could easily go over the yield stress without stopping or correcting for it.

The 'Evolutionary Structural Optimization' (ESO) [25] is only capable of removing inefficient material. The difference with the 'Bi-directional Evolutionary Structural Optimization' (BESO) [21] is that the latter is also allowed to include elements after they have been rendered idle. This makes it converge faster than the ESO. Another difference is that the BESO

method can be started by only filling in the least amount of elements, connecting the nodes where the force is applied to the kinematically constrained nodes. From there the structure can grow to the desired shape and remove elements that helped to create that shape.

$$\begin{aligned} \sigma_{VM,e} &\leq RR \cdot \sigma_{VM,max} \quad with \quad RR = r_1 \cdot SS + a_{RR} \cdot ON \\ \sigma_{VM,e} &\geq IR \cdot \sigma_{VM,max} \quad with \quad IR = 1 - i_1 \cdot SS - a_{IR} \cdot ON \end{aligned} \tag{2.11}$$

Where RR is the rejection ratio, IR is the inclusion ratio, $\sigma_{VM,e}$ is the Von Mises stress in the element and $\sigma_{VM,max}$ is the maximum allowable Von Mises stress. These are factors between 0 and 1 which will be the condition whether an element is removed or included.

SS is the steady state number, which is incremented by 1 every time a steady state has been reached. That happens when no elements are added or removed. The ON is the Oscillation Number, which is also incremented by 1, but only when an element has been included and removed in subsequent iterations. Furthermore, r_1 and i_1 are determined on experience and in the paper [25] the values of $r_1 = 0.001$ and $i_1 = 0.01$ are recommended. The a_{RR} and a_{IR} are constants as well and also established on experience and are recommended to be set at $a_{RR} = 0.01$ and $a_{IR} = 0.1$.

The iteration loop is similar to the one for SIMP:

1. calculate Von Mises stress for each element
2. check whether it should be included, excluded or should stay the same. This is determined whether the stress in the element is lower than the $RR \cdot \sigma_{VM,max}$ or higher than $IR \cdot \sigma_{VM,max}$
3. set this value for next iteration
4. check whether steady state has been reached. If that is the case SS should be incremented with 1.

That vector consists of values between 0 and 1 and are multiplied with the E modulus of each element. When it is close to 0, the element is regarded as removed and when it is 1 the element is included. To keep track of the performance, the following formula is used:

$$f = PI = \frac{\sum_{e=1}^{n} \sigma_{VM,e} V_e}{FL} \tag{2.12}$$

This objective function is equal to its Performance Index (PI) where V_e is the element volume, F is the input force and L represents the length of the structure This is a non-dimensional number that must be minimized. It must be kept in mind that this objective function merely describes the performance of the geometry, but is not influenced by an optimization algorithm. It is a result from what happens with the rejection and inclusion ratios.

2.3.3. Comparison

So the main difference between the two optimization methods is the sensitivity analysis. Where the SIMP evaluates a function and uses an optimization algorithm to find the density factor where the sensitivity becomes 0, the BESO method is more crude by assuming a threshold of inclusion or rejection ratio of the yield stress. The sensitivity analysis of the SIMP can become a problem with a model that contains a lot of elements as it is computational more expensive to find where the sensitivity becomes zero. Another difference is that with the SIMP method, the element can have a virtual density, resembling not a realistic material but by homogenization it should resemble part void, part material.

Both optimization types require human input, rendering them heuristic. SIMP requires a penalization factor and the evolutionary methods need the ratios set. Both the authors seem to have a discussion about which one yields the best results, both having criticism toward the other method about how much human input is needed [24].

2.3.4. Conclusion

With the two optimization approaches the results are satisfactory as well as the amount of iterations. Where they do differ however, is the applicability to large problems regarding the computational expense. SIMP requires one function evaluation and a root search for the sensitivity, while the BESO method only requires an if statement per element to check whether it should be an idle element or material. Since the midsection of the TSHD is a large problem, the choice is evident to be for the BESO method. With the welcome advantage that the method is simple in nature, so could easily be adapted and probably even improved.

2.4. Shape and Topology Optimization in Ship Structures

To find out how this research will compare to the current state of ship structure optimization, a review of relevant and recent papers has been conducted.As can be found in the 20th International Ship and Offshore Structures Congress (ISOSC) optimization is starting to be incorporated into the ship design methods more frequently in recent years [23].

Kim et al. (2017) [7] have used a steepest descent algorithm to find a layout and sizing of stiffened panels for a semi-submersible floater. The objective for this shape optimization was to minimize the weight and the constraints consisted out of buckling and yield assessments. These constraints were calculated with a rule based system.

Garbatov and Goergiev (2017) [6] have set up a multi objective nonlinear optimization where a reliability-based design optimization is combined with a Pareto frontier. The objectives applied were a minimal net sectional area and a minimal deflection of a panel with a single stiffener. The loads employed were based on a panel with lateral hydrostatic and global membrane loads, resembling a keel plate of a ship.

Tschullik et al. (2010) [22] has used the SIMP method to find an optimal topology for the double bottom layout in a container ship. Much as the same reasons this research concerns a midsection of a ship; high repeatably so an improvement could have a large effect on the total mass of the ship. Two optimizations were executed, one starting with the conventional holes in the floor and another one that was completely free to create a desired geometry. Mass reductions of 11% for the conventional hole start and 38% for the less restricted optimization were acquired. Next to the mass decrease a higher utilization, so higher average stress in the active material were the result. On top of that, it is stated that topology optimization could be used in the early stages of the design process to have more efficient material and to reduce the amount of iteration steps in a later stage of the design as a near optimum has been reached in the beginning already.

Leidenfrost et al. (2016) [10] have used topology optimization to find the optimal arrangement for stiffeners in a 46 meter sailing yacht. This shows that the conventional method of having all the stiffeners and web frames in a orthogonal layout is most probably not the optimum in weight. In this paper the topology optimization results were also subject to an ‘abstraction’ process where the fully organic geometries were transformed to more producible shapes like stiffeners. Resulting in Figure 2.5.

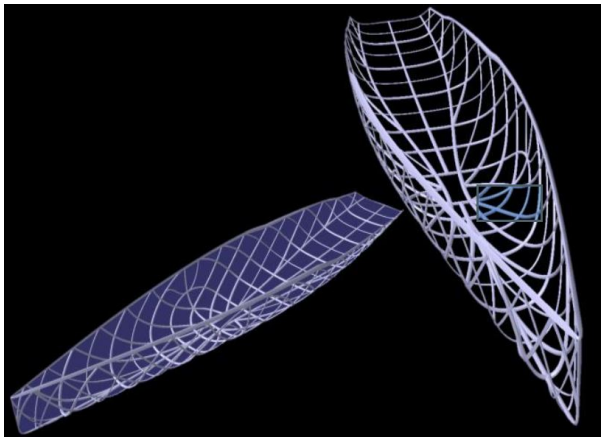

Figure 2.5: Result of topology optimized stiffener layout [10].

From these examples it can be concluded that ship structure optimization is currently a topic of interest. These researches have applied either a shape or topology optimization but have not combined the two and applied the methods.

3
Research Objectives

3.1. Research Questions

How can a shape and topology optimization with buckling and yield constraints help design the midsection of a TSHD?

3.2. Research Subquestions

To answer the main question, five sub questions have been defined to answer the main research question.

1. *How can the longitudinal stiffener layout of a ship midsection be optimized?*
   The stiffened panels that make up the outer hull are subjected to two types of loads; a global stress and local loads. Global stresses are induced by a bending moment as a result of a unbalance in buoyancy and weight distribution throughout the length of the ship. The local loads are the water pressure on the hull and a pressure in the hopper created by the sludge. A modelling strategy is sought for that optimizes ships that are subjected to these loads, based on minimum ship mass.

2. *How to optimize the transverse web frame of a ship?*
   Transverse web frames are subjected to local loads, which are introduced to the stiffened panels and transferred to the web frame. These transverse web frames are optimized to minimize ship mass. A modified BESO method will be applied to find the a feasible and improved topology.

3. *What is the interaction between shape optimization and topology optimization?*
   Based on shape optimization, longitudinal stiffened panels are designed. If stiffened panels of the ship hull have different stiffness values, they will deflect differently. It is hypothesized that this will result in varying web frame topologies that are obtained with topology optimization. The interaction between the two optimization steps is explored.

4. *What is the optimal web frame spacing for an optimized web frame topology combined with an optimal longitudinal stiffener layout for a given length of a midsection?*
   The web frame spacing defines the total local load in each stiffened panel and therefore in each web frame. An optimum is sought between lighter stiffened panels and web frame topologies distributed across shorter distances, and stiffer, heavier panels and web frames with larger web frame spacing.

5. *How can optimization techniques be used for a better understanding of ship structures?*
   News ships are often designed based on existing ship designs that meet requirements of the client and have been tested and proven. This research aims at better understanding ship structures using optimization methods, to possibly guide new lines of research and enhance the ship design process.

3.3. Methodology

1. *How can the longitudinal stiffener layout of a ship midsection be optimized?*
   A computationally efficient analytical model is assembled to obtain a first overview of a well performing layout of longitudinal stiffeners and plate thicknesses. 5,000,000 randomly generated midsections are analyzed with the analytical model. The top 100

analytical solutions are selected and run with a numerical model.

The yield and buckling constraints calculated with the analytical model will be checked immediately and when these are violated it will receive a 'false' fitness, rendering them out of the final solutions. All solutions are stored and later filtered so that a set of feasible designs is kept. The top performing solutions of the analytical and numerical solutions will be compared and the one with the best fitness will be passed on to the next model to find a matching web frame with topology optimization.

2. *How to optimize the transverse web frame of a ship?*
   The existing BESO method is modified to suit a topology optimization of this scale and relatively complex loading. This method will first undergo a bench marking process to verify that the modified BESO method performs well enough to be able to apply it. Next to that, an equivalent web frame thickness has to be determined to compensate for the fact that this optimization does not include flanges on the web frames, which is often the case in existing ships. Consecutively, the results from the previous step will be used to find a web frame suited for this longitudinal stiffener arrangement.

3. *What is the interaction between shape optimization and topology optimization?*
   Since topology optimization is extremely sensitive to model changes, it is expected that when the stiffness of the surrounding plates changes, the topology will also be different. A case study is conducted on one specific web frame spacing, comparing outcomes of runs where all stiffened panels have the same stiffness and model outcomes of runs where all stiffened panels have a distinct thickness.

4. *What is the optimal web frame spacing for an optimized web frame topology combined with an optimal longitudinal stiffener*
   Midsections with seven distinct web frame spacings are input for the optimization procedure (shape optimization for longitudinal stiffened panels and topology optimization for transverse web frames). To be able to compare results, the total weight of the obtained shape is divided by the web frame spacing. It might be better to have many small web frames with lighter longitudinal stiffening or the exact opposite; a few large web frames with heavy stiffened panels and large span.

5. *How can optimization techniques be used for a better understanding of ship structures?*
   The optimization procedures can show underlying mechanisms in the structure that are not evident on first glance.

II

Models and Results

4
Stiffened Panel Model

4.1. Introduction

An analytical stiffened panel model can make a good approximation of what the actual stresses will be. However, it is hard to include stresses other than the lateral pressure and longitudinal stress. Therefore, after the analytical optimization has ran, the best results have to be checked with a numerical model.

4.2. Geometry

A reference ship was used to provide the optimization with realistic loading and a representative geometry. The full and the altered geometries are shown in Figure 4.1.

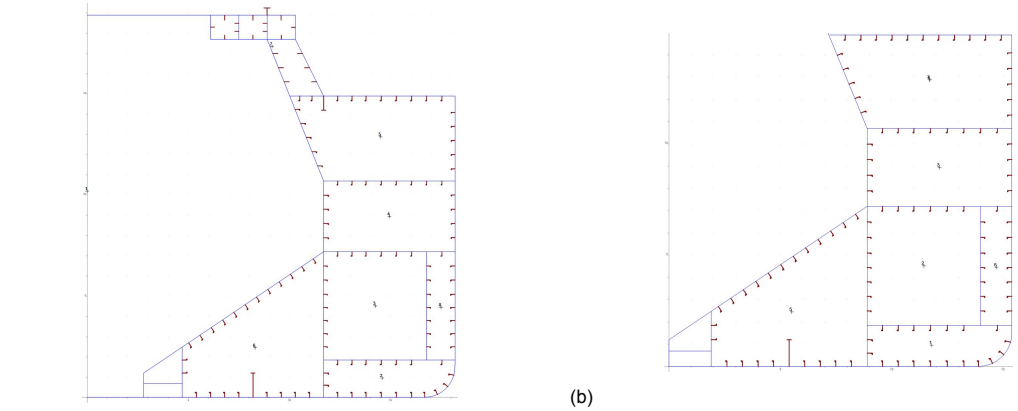

(a) (b)

Figure 4.1: Original ship and the altered version.

To keep the model straightforward, the coaming was removed from the original ship and to be able to parameterize the structure, a few simplifications have been made.

1. To approach the actual structure, the bilge has been divided into two plates. Because these plates are relatively small, one stiffener of variable geometry is assigned to them.
2. The plate thicknesses for the lower hopper plates are in reality not constant. The lateral pressure in the bottom of the hopper is larger than at the top. For this model the plate is taken as one item and therefore this plate thickness and stiffener arrangement is constant over that length.

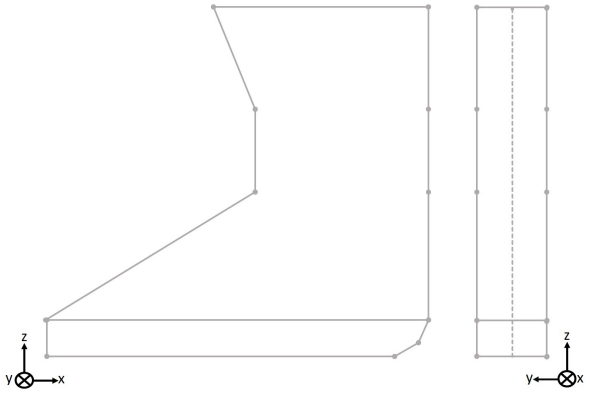

Figure 4.2: Simplified geometry representation.

4.3. Loading

A global hull analysis report based on ship rules by BV was used to determine the loads. For the global loading the absolute values for hogging and sagging were established by adding the still water and wave loads. The report was based on the full geometry with the coaming. When the coaming is removed, a lot of the stiffness is discarded as well. Therefore the global bending moment has to be scaled. The original moment of inertia was 122.41 $[m^4]$ and according to MARS2000 the new moment of inertia is 51.64 $[m^4]$. So the scaling factor for the bending moment becomes $SC_{BM} = \frac{51.64}{122.41}$ The maximum water pressure also differs in hogging and sagging ($(W_{max,hog}, W_{max,sag})$, but the hopper load H_{max} does not change. These resulted in:

item	value	unit
$M_{sw,sag}$	3491329	[kNm]
$M_{wv,sag}$	1438210	[kNm]
$M_{tot,sag}$	4929371·SC_{BM}	[kNm]
$W_{max,sag}$	0.0975	[MPa]
$M_{sw,hog}$	1348658	[kNm]
$M_{wv,hog}$	1341653	[kNm]
$M_{tot,hog}$	2690311·SC_{BM}	[kNm]
$W_{max,hog}$	0.1498	[MPa]
H_{max}	0.2486	[MPa]

Table 4.1: Load input (absolute values)

(a) (b)

Figure 4.3: Maximum sagging (a) and maximum hogging (b) loading condition.

4.4. Geometry Variables

To create a midsection out of stiffened panels in a random way, upper and lower bounds have to be set from which the geometry can be made out of. All eleven panels described in

Section 4.2 consist out of T-stiffeners and a plate. A visualization is shown in Figure 4.4 and the range and steps in which the variables are selected are depicted in Table 4.2.

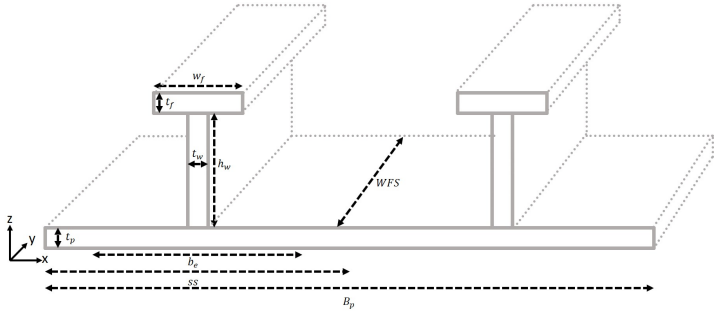

Figure 4.4: Visualization of a stiffened panel and its geometry

	t_w $[mm]$	w_f $[mm]$	h_w $[mm]$	t_f $[mm]$	t_p $[mm]$	n_s $[-]$
min	4	$t_{w,max}$	50	5	10	3
max	24	500	700	24	30	20
step	2	10	10	2	2	1

Table 4.2: Constraints on generating SOV.

This results in a total of 365,615,000 possible midsection stiffener arrangements.

4.5. Analytical Model

A quick way of assessing a lot of options is to analyze the panels analytically. These will later be checked with a FE analysis.

4.5.1. Moment of Inertia

To define the stresses, the moment of inertia has to be determined. That is done by determining the inertia of the plate, webs and flanges and adding them together. When the stiffness of the plate stiffener combination has been determined, it has to be transformed to the correct location in the geometry.

$$I_{x,p} = \frac{B_p \cdot t_p^3}{12} \quad , \quad I_{z,p} = \frac{t_p \cdot B_p^3}{12} \tag{4.1}$$

$$I_{x,w} = \frac{t_w \cdot h_w^3}{12} \quad , \quad I_{z,p} = \frac{h_w \cdot t_w^3}{12} \tag{4.2}$$

$$I_{x,f} = \frac{w_f \cdot t_f^3}{12} \quad , \quad I_{z,p} = \frac{t_f \cdot w_f^3}{12} \tag{4.3}$$

$$c_{x,p} = \frac{B_p}{2} \quad , \quad c_{z,p} = \frac{t_p}{2} \tag{4.4}$$

The vector $[sv]$ holds the location of the center of the web and flange of a stiffener on a plate. For example, with a plate of 1000 [mm] wide and three stiffeners, the spacing vector (sv) would be $sv = [250, 500, 750]$.

$$c_{x,w} = [sv] \quad , \quad c_{z,w} = t_p + \frac{h_w}{2} \tag{4.5}$$

$$c_{x,f} = [sv] \quad , \quad c_{z,f} = t_p + h_w + \frac{t_w}{2} \tag{4.6}$$

Once the local centroids of each component of the stiffened panel has been determined, the centroid c_{ps} and moments of inertia I_{ps} of the complete panel can be established.

$$c_{z,ps} = \frac{A_p \cdot z_p + n_s \cdot (A_w \cdot c_{z,w} + A_f \cdot c_{z,f})}{A_p + n_s \cdot (A_w + A_f)} \tag{4.7}$$

$$c_{x,ps} = \frac{A_p \cdot x_p + \sum_{i=1}^{i=n_s} (A_w \cdot c_{x,w} + A_f \cdot c_{x,f})}{A_p + n_s \cdot (A_w + A_f)} \tag{4.8}$$

$$I_{xx,p} = I_{x,p} + A_p \cdot (c_{z,p} - c_{z,ps})^2 \tag{4.9}$$

$$I_{zz,p} = I_{z,p} + A_p \cdot (c_{x,p} - c_{x,ps})^2 \tag{4.10}$$

$$I_{xx,s} = I_{x,w} + A_w \cdot (c_{z,w} - c_{z,ps})^2 + I_{x,f} + A_f \cdot (c_{z,f} - c_{z,ps})^2 \tag{4.11}$$

$$I_{zz,s} = I_{z,w} + A_w \cdot (c_{x,w} - c_{x,ps})^2 + I_{z,f} + A_f \cdot (c_{x,f} - c_{x,ps})^2 \tag{4.12}$$

$$I_{xx,ps} = I_{xx,p} + n_s \cdot I_{xx,s} \tag{4.13}$$

$$I_{zz,ps} = I_{zz,p} + \sum_{i=1}^{i=n_s} I_{zz,s} \tag{4.14}$$

$$\begin{aligned} I_{xz,ps} = {} & A_p \cdot (c_{x,p} - c_{x,ps}) \cdot (c_{z,p} - c_{z,ps}) \quad + \\ & n_s \cdot (A_w \cdot (c_{x,w} - c_{x,ps}) \cdot (c_{z,w} - c_{z,ps}) + A_f \cdot (c_{x,f} - c_{x,ps}) \cdot (c_{z,f} - c_{z,ps})) \end{aligned} \tag{4.15}$$

When the information of all stiffened panels have been calculated, the next step can be made. The centroids and moments of inertia are all with respect to the horizontal x-axis and not with respect to each other, resembling the complete midsection. To change the properties, two procedures are taken. The first is to rotate the stiffened panel around its centroid in the correct orientation and secondly it has to be translated to the corresponding x- and z-location. To rotate the panel around the origin, the following formulas are applied.

$$I_{u,ps} = \frac{I_{xx,ps} + I_{zz,ps}}{2} + \frac{I_{xx,ps} - I_{zz,ps}}{2} \cdot cos(2\theta) - I_{xz,ps} \cdot sin(2\theta) \tag{4.16}$$

To create the inertia moment of the full midsection, all the areas and relocated centroids are used to find the centroid $c_{z,mid}$ and finally the respective moments of inertia are added to create $I_{xx,mid}$. The global bending moment that is applied in these models is only around the x-axis and therefore to determine and approach the membrane stress on each panel, only the $I_{xx,mid}$ is required.

$$I_{xx,ps,trans} = I_{u,ps} + A_{ps} \cdot (c_{z,ps,trans} - c_{z,mid})^2 \tag{4.17}$$

$$I_{xx,mid} = \sum I_{xx,ps,trans} \tag{4.18}$$

With this the local membrane stress induced by the global bending moment at the centroid can be estimated for each plate-stiffener combination.

$$\sigma_{BM,loc} = \frac{M_{global} \cdot (c_{z,ps,trans} - c_{z,mid})}{I_{xx,mid}} \tag{4.19}$$

4.5.2. Yield

To follow the hierarchy of how stress is introduced into the structure, it makes sense to start with checking whether the plate between the stiffeners will yield or not. The orientation and loading is visualized in Figure 4.6 and the supporting equations are provided below. The maximum stress induced by the lateral load on the plate between the stiffener is analyzed, followed by the complete stiffened panel between the web frames which is simplified to a column. For the keel plate the pressures p1 and p2 are identical, but for the hopper and side hull these have a varying pressure. The plate between the stiffeners that will be subjected to the most lateral stress is considered for the plate calculation. The orientation for the column calculation is different and the p1 and p2 would be constant over this axes. The average between p1 and p2 are taken to have the same total force put on the column.

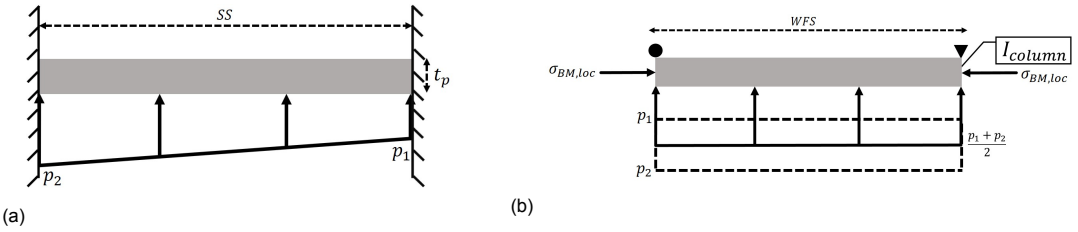

Figure 4.5: (a) plate between stiffeners and (b) column between web frames

$$I_{x,plate} = \frac{WFS \cdot t_p^3}{12} \tag{4.20}$$

$$M_{max,plate} = \frac{WFS \cdot ss^2}{12} \cdot \frac{p1 + p2}{2} \tag{4.21}$$

$$\sigma_{max,plate} = \frac{M_{max,plate} \cdot \frac{t_p}{2}}{I_{plate}} \tag{4.22}$$

$$I_{column} = I_{xx,ps} \tag{4.23}$$

$$c_{column} = max\{(t_p + h_w + t_f) - c_{z,ps}, \quad c_{z,ps}\} \tag{4.24}$$

$$M_{max,column} = \frac{B_p \cdot WFS^2}{16} \cdot \frac{p1 + p2}{2} \tag{4.25}$$

$$\sigma_{max,column} = \frac{M_{max,column} \cdot c_{column}}{I_{column}} + \sigma_{BM,loc} \tag{4.26}$$

4.5.3. Linear Buckling

To assess the buckling analytically two situations are observed, the plates between the stiffeners and the plate-stiffener combination simplified as a column.

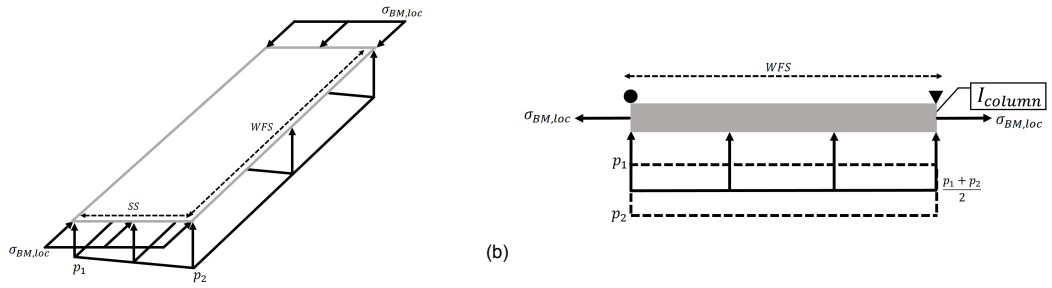

Figure 4.6: (a) plate between stiffeners and (b) column between web frames

The Euler buckling load for the plate and column is determined with the following set of formulas. The orientation of the plate and column are similar to the previously defined yield analyses. The equations are based on Chapter 12 of Ship Structural Analysis and Design by Paik [18].

$$D = \frac{E \cdot t_p^3}{12 \cdot (1 - \nu^2)} \tag{4.27}$$

$$\sigma_{E,plate} = \frac{\pi^2 \cdot D}{t_p \cdot ss^2} \tag{4.28}$$

$$\sigma_{E,plate} = C_{px} \cdot \frac{\pi^2 E}{12(1-\nu)^2} \cdot \left(\frac{t_p}{ss}\right)^2 \cdot K \cdot \eta \quad with \quad K = 4 \tag{4.29}$$

$$where \quad \eta = \begin{cases} 1 & \sigma_{E,plate} \leq \sigma_Y/2 \\ \frac{\sigma_Y}{\sigma_{E,plate}} - \frac{1}{4}\left(\frac{\sigma_Y}{\sigma_{E,plate}}\right)^2 & \sigma_{E,plate} > \sigma_Y/2 \end{cases} \tag{4.30}$$

$$and \quad C_{px} = \begin{cases} 1 + \frac{1}{576} \cdot \left(\frac{p \cdot ss^4}{E \cdot t_p^4}\right)^{1.6} & if \quad \frac{WFS}{ss} \geq 2 \\ 1 & else \end{cases} \tag{4.31}$$

$$\beta = \frac{b_p}{t_p} \cdot \sqrt{\frac{\sigma_Y}{E}} \tag{4.32}$$

For column buckling it is important to first find the effective width for a plate-stiffener combination, as the stress is not distributed equally throughout the plate. The following equations are used to find the effective buckling load σ_{xu}. These are based on the book Ultimate Limit State Design by Paik [20].

$$b_e = \begin{cases} b_p & \beta \leq 1 \\ \left(\frac{2}{\beta} - \frac{1}{\beta^2}\right) \cdot b_p & \beta > 1 \end{cases} \tag{4.33}$$

$$\sigma_{xE} = \frac{\pi^2 \cdot E \cdot I_e}{WFS^2 \cdot A_{ps}} \tag{4.34}$$

$$\sigma_{xu} = \begin{cases} \sigma_{xE} & \sigma_{xE} \leq \sigma_Y/2 \\ \frac{\sigma_Y}{\sigma_{xE}} - \frac{1}{4}\left(\frac{\sigma_Y}{\sigma_{xE}}\right)^2 & \sigma_{xE} > \sigma_Y/2 \end{cases} \tag{4.35}$$

The buckling load must not be exceeded by the load put on the beam. That is a combination of both an axial stress by the global bending moment and a lateral load because of the water or hopper pressure. Using buckling and yield as optimization constraints is in line with the research conducted by Kim et al.[7]

$$P_E = \frac{\pi^2 \cdot E \cdot I_{e,colunm}}{WFS^2} \tag{4.36}$$

$$\sigma_{c,column} = \sigma_{BM,loc} + \left(\frac{B \cdot WFS^2}{16} + \frac{\sigma_{BM,loc} \cdot A_{ps}}{1 - \frac{\sigma_{BM,loc} \cdot A_{ps}}{P_E}} \cdot \frac{5 \cdot WFS^4}{768 \cdot E \cdot I_{column}} \right) \cdot \frac{p1 + p2}{2} \cdot \frac{c_{column}}{I_{column}} \tag{4.37}$$

4.5.4. Constraints

Now that all the loads can be calculated, the constraints can be set up.

$$g_1 = \frac{\sigma_{max,plate}}{\sigma_Y} \tag{4.38}$$

$$g_2 = \begin{cases} \frac{\sigma_{max,column}}{\sigma_Y} & if \quad \sigma_{BM,loc} \geq 0 \\ \frac{\sigma_{c,column}}{\sigma_{xu}} & if \quad \sigma_{BM,loc} < 0 \end{cases} \tag{4.39}$$

$$g_3 = \frac{\sigma_{BM,loc}}{\sigma_{c,plate}} if \quad \sigma_{BM,loc} < 0 \tag{4.40}$$

All constraints must be $g_i \leq 1 \cdot CR$ to pass. CR is the constraint relaxation. In some cases it might be better to relax constraints that are generally too conservative.

4.5.5. Simulated Annealing

For this analytical optimization problem, the simulated annealing algorithm is used. This prevents the sheer amount of data that will be created because the amount of results will not be exactly the given amount of iterations. The fitness function and constraint evaluation are represented by F(x) and G(x) respectively.

$$\begin{aligned}
C &= x_{random} \\
F_{current} &= F(C) \\
G_{current} &= G(C) \\
&for \quad T \quad in \quad range(T_{max}, \quad T_{min}, \quad n_{iterations}) \\
&\quad N = x_{random} \\
&\quad F_{new} = F(N) \\
&\quad G_{new} = G(N) \\
&\quad if \quad g_1, g_2, g_3 \geq 1 \cdot CR \\
&\quad\quad F_{new} = false \\
&\quad \Delta F = F_{current} - F_{new} \\
&\quad if \quad (\Delta F > 0) \\
&\quad\quad F_{current} = F_{new} \\
&\quad\quad C = N \\
&\quad elseif \quad \left(e^{\frac{\Delta F}{T}} > random(0,1) \right) \\
&\quad\quad F_{current} = F_{new} \\
&\quad\quad C = N \\
&\quad else \\
&\quad\quad C = C \\
&\quad endif \\
&endfor
\end{aligned}$$

Another approach would be to keep making new set of variables (SOV) until it passes the constraints but with a while-loop it is not possible to define a time in which the optimization will be done. For the higher WFS, the constraints were violated so many times that it could run for a long time without giving results, surpassing the goal of this optimization.

4.5.6. Optimization Procedure

For this optimization the constraint relaxation CR was set to $CR = [1.25, 1.05, 1.05]$ to avoid disregarding too many solutions due to conservative constraints. The parameters used are: $T_{max} = 10000 \cdot WFS_{ratio}$, $T_{min} = 0$ and finally $n_{iterations} = 5,000,000$ which would take approximately 14 hours to compute. The scores are sorted and the top 100 solutions will undergo the numerical procedure as described in Section 4.6. This way it is possible to compare them and it gives a check whether the constraints applied have been sufficient.

4.6. Numerical Analysis of Analytical Solutions

The optimization has evaluated 5 million solutions and kept the 100 best and now these will undergo a numerical analysis which incorporates all the interactions of the loads. The loading is applied in the same manner as depicted in Figure 4.3, but for the FEM analysis it also needs kinematic constraints as shown in Figure 4.7. An infinitely stiff web frame is modeled by applying the constraints in the middle of the structure. The orange arrows show rotational constraints on the location where the ship in reality continues. This satisfies the fact that no rotation around the x and z directions are possible because that is the middle of the plate where the moment and displacement are maximal but rotation is zero. The applied element size is 150 [mm].

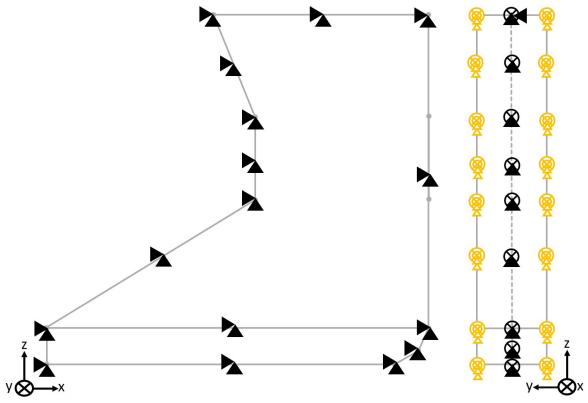

Figure 4.7: Plate-stiffener numerical model constraints.

After the 100 iterations have been numerically analyzed, the data is filtered to satisfy the constraints of $\sigma_{VM,max} \leq 235[MPa]$ and $BF_{min} \geq 2.5[-]$. The buckling factor is derived by letting Ansys find the first 20 buckling modes and sorting for the lowest positive factor.

4.7. Results

In Figure 4.8 the optimal stiffened panel layouts are depicted for each web frame spacing. The thicknesses of the plate, web and flange are not included as the scale is too small for display. The masses, maximum stresses and minimal buckling factors are shown in Table 4.3 which is followed by Table 4.5 that shows the ratios of the constraint violations of the 5,000,000 iterations.

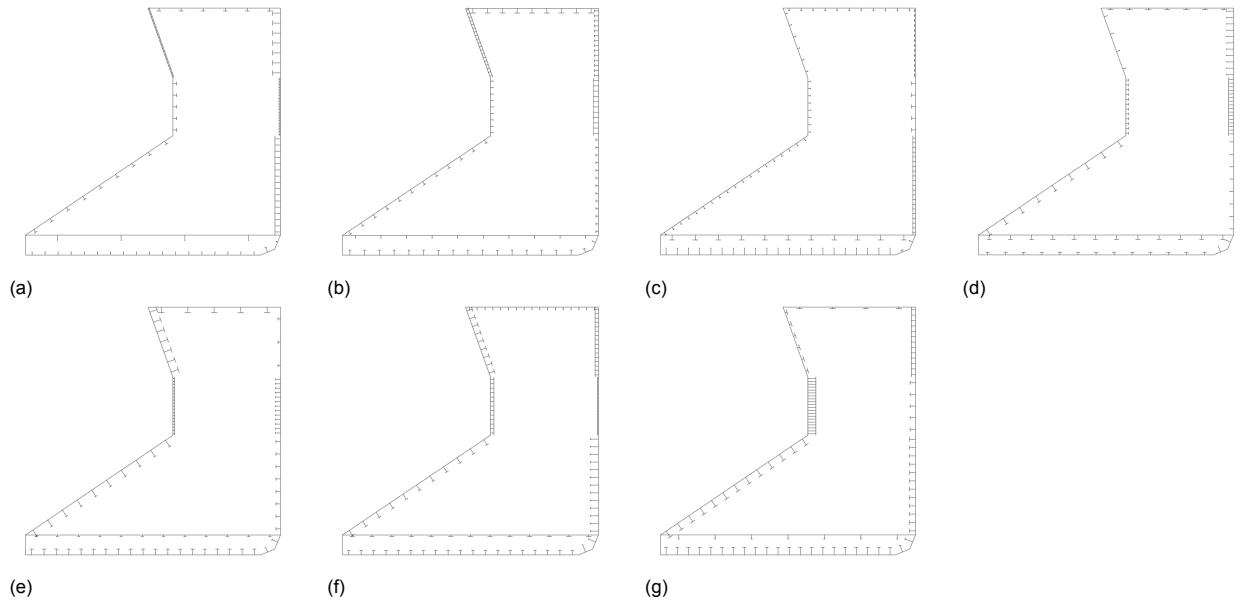

Figure 4.8: Shape optimization results of WFS = (a) 562.5 [mm] (b) 1125 [mm] (c) 1687.5 [mm] (d) 2250 [mm] (e) 2812.5 [mm] (f) 3375 [mm] (g) 3937.5 [mm]

WFS [mm]	562.5	1125	1687.5	2250	2812.5	3375	3937.5
mass [t]	5.62	11.05	17.73	26.03	32.64	40.56	59.02
$\sigma_{VM,max,sag}$[MPa]	88.37	101.85	62.27	113.68	98.03	135.52	154.04
$\sigma_{VM,max,hog}$ [MPa]	48.71	101.18	63.49	182.08	124.76	136.11	150.60
BF_{sag} [-]	4.59	3.34	3.59	4.69	4.71	3.32	3.94
BF_{hog} [-]	8.46	2.63	2.91	-8.57	-8.37	-6.09	8.54

Table 4.3: Mass, maximum Von Mises stress and buckling factor of the best results.

4.8. Discussion

4.8.1. Constraint Influence

Table 4.4 shows the influence of each of the constraints for the analytical optimization.

WFS [mm]	562.5	1125	1687.5	2250	2812.5	3375	3937.5
g_1	0.213	0.213	0.213	0.213	0.213	0.213	0.213
g_2	0.002	0.032	0.095	0.172	0.254	0.335	0.408
g_3	0.149	0.149	0.149	0.149	0.149	0.149	0.149
total	0.363	0.394	0.460	0.534	0.616	0.697	0.769

Table 4.4: Ratio of declined solutions and constraint contribution

The first and third constraint seem to be constant for all the seven different web frame spacings. The consistency of g_1 can be explained by the fact that total lateral load increases linearly with the web frame spacing and so does the stiffness of the beam that resembles the plate as shown in Figure 4.6 and equations 4.20, 4.21 and 4.22.

The third constraint has the same quality as the global load is constant and the buckling load of the plate in this model is regarded as not dependent on the length of the plate. This is not realistic as especially with smaller web frame spacings, the plate 'orientation' changes and the long side is the one along the web frame and the short side is attached to the stiffeners. This is a shortcoming of the analytical model that should be noted.

4.8.2. Differences Analytical and Numerical Results

The fact that not all the analytical solutions will be accepted after the numerical simulation is because the numerical solution is a lot closer to the reality and the effects of transverse stresses induced by the hydrostatic pressures form the hopper and hull are incorporated into this design. To overcome the denial rate after the numerical analysis, a direct numerical approach was also used. However, the results were not sufficient as in the same time the analytical will produce 5,000,000 solutions the numerical is only capable of 1000. That is not enough to find a good solution, however it can get lucky and find one that is better but the probability of this happening is not high. Another disadvantage of the direct numerical analysis is that the calculation time is geometry dependent. As the web frame spacing increases, so do the number of elements and that will lead to a long computing time. The analytical analysis is not sensitive to the size of the geometre. A detailed description of the direct numerical analyisis is given in Appendix A.

WFS [mm]	562.5	1125	1687.5	2250	2812.5	3375	3937.5
$\sigma_{VM,max,sag}$ [MPa]	0	1	0	0	1	2	1
$\sigma_{VM,max,hog}$ [MPa]	0	0	2	3	4	10	6
BF_{sag} [-]	45	53	59	51	55	53	18
BF_{hog} [-]	34	48	61	30	44	42	14
total [-]	100	100	100	100	100	100	61
declined [-]	45	57	72	51	58	59	23

Table 4.5: Number of declined solutions after numerical analysis.

From Table 4.5 it is evident that the yield constraint is almost never violated in the numerical model if it passed the analytical constraints. If the analytical procedure was more elaborate by also including the transverse stresses, bending and buckling of stiffener webs and flanges and if the constraint relaxation was tuned perfectly all the solutions generated by the analytical model would also pass the numerical analysis. However, if the analytical model is too conservative it could be possible that some solutions do not satisfy the analytical constraints, but would pass the numerical one thus leaving out perfectly good solutions. It is likely that the yield constraints are set conservative in the analytical model. The buckling load calculated by the analytical model is the main reason why some analytical solutions are not passing to be the best solution.

Another aspect that is striking when the information for the web frame spacing of 3937.5 in Table 4.4 is that the probability of passing the constraints with a random set of panels and stiffeners is 23.1%, but only 61 solutions were viable from the analytical approach. This is due to the fact that even when a viable option has been randomly created, it would also have to pass the objective comparison. In other words, if it passes the constraints but is heavier than the previous iteration it will only be accepted if the SA algorithms accepts it.

4.8.3. Trends in Stiffened Panels

The hope was that the shape optimization would give a unambiguous answer to how the ship should be longitudinally stiffened. Examples of these would be a common plate thickness or amount of stiffeners per local panel and a recorruing web height to flange width ratio. Table 4.6 shows the panel dimensions of the keel plates of the seven final results. However, these geometry results do not show a definite amount of resemblance.

WFS [mm]	562.5	1125	1687.5	2250	2812.5	3375	3937.5
$t_w[mm]$	12	4	10	22	8	16	24
$w_f[mm]$	45	125	35	245	215	185	205
$h_w[mm]$	180	300	410	160	350	270	450
$t_f[mm]$	10	12	14	24	14	18	8
$n_s[-]$	18	16	21	13	19	19	21
$t_p[mm]$	30	18	22	28	28	22	21

Table 4.6: Keel plate dimensions of SO results.

With the lack of geometrical parallels, the moments of inertia and area have been calculated for three different panels that are each in a different load state, the keel, the vertical part of the hopper and the main deck.

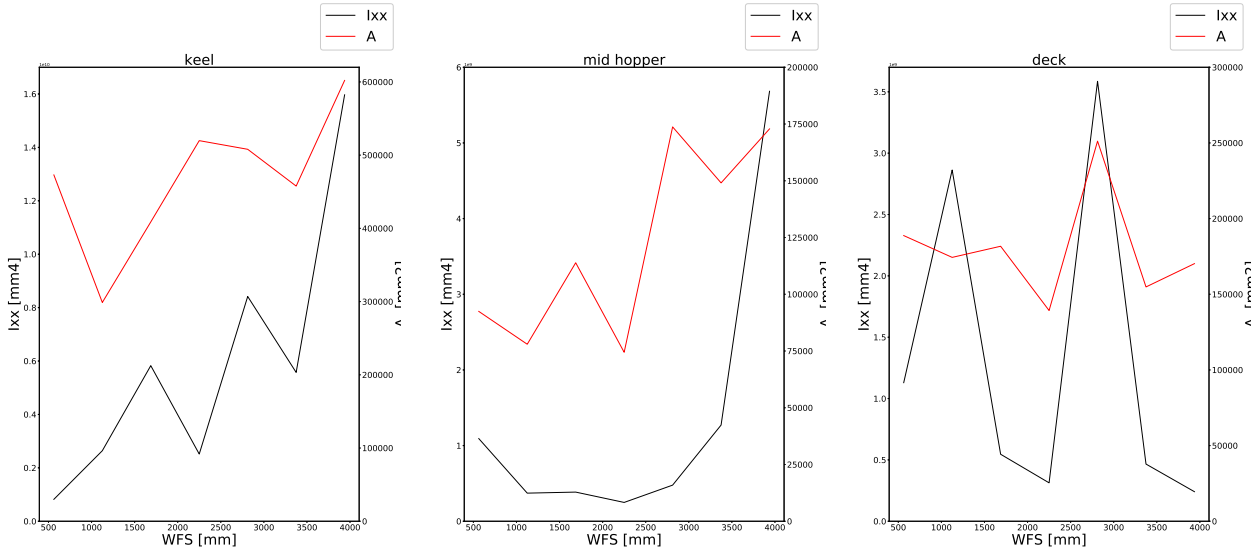

(a) (b) (c)

Figure 4.9

	WFS [mm]	562.5	1125	1687.5	2250	2812.5	3375	3937.5
keel	$I_x[mm^4]$	820895520	2641038202	5826674143	2516321180	8416891587	5573674633	15969073527
	$A[mm^2]$	472980	298800	408790	519800	507990	457750	602040
mid hopper	$I_x[mm^4]$	1092463370	371567606	385293779	248706157	477420866	1271121432	5682777119
	$A[mm^2]$	92450	77980	113880	74440	173732	149064	172860
deck	$I_x[mm^4]$	1129284551	2862954560	546045794	313084838	3586039508	465994350	240769422
	$A[mm^2]$	188780	174370	181730	139260	251200	154840	170240

Table 4.7: Moments of Inertia and Area of best solution panels

It is hard to find trends in this model. Due to the large amount of variables and therefore possibilities, it is better to see these solutions as improved designs rather than the optimal result. A weak increase is seen in the panels that have a hydrostatic pressure, which makes sense as this increases with the web frame spacing. The main deck should, however show some resemblance as the global load does not vary as much. The global load for each panel varies per solution as the neutral axis shifts, but the enormous fluctuating behaviour is too much to settle on a trend.

4.8.4. Numerical Procedure

As the element size is 150 [mm], it is not guaranteed that all the webs of the stiffeners have at least 3 elements in height. That could give it a higher stiffness than that it actually would have. It cannot properly calculate the shear that would go through the web and therefore

overestimate the buckling load. The same applies for the flanges and this should be kept in mind while assessing the results.

The infinitely stiff web frame that is resembled by the kinematic constraints in the middle of the model will also overestimate the actual stiffness of the structure. This effect diminishes as the web frame spacing increases, but it will still be a factor. This over-estimation should also be kept in mind when assessing the results.

5
Web Frame Model

5.1. Introduction
The goal of this model is to find a lightweight web frame that can withstand all the local loads. The hopper load and water pressure introduce stress on the stiffened panels, which in turn are reinforced by the transverse web frames.

The applied algorithm will be described and verified, after that the geometry, loading and optimization procedure are shown.

5.2. Modified BESO
5.2.1. Neighbour Inclusion Ratio
The basis for the algorithm was the BESO method as described in Section 2.3.2. It is slightly modified for a possible faster convergence and to be able to cope better with unmapped meshes. BESO differs from ESO that it is able to revive turned off elements, and with this alteration MBESO takes that concept one step further. It also allows the neighbouring elements to be reactivated. This way, in extreme local stress situations a lot of material is added in one iteration and therefore reducing the stress.

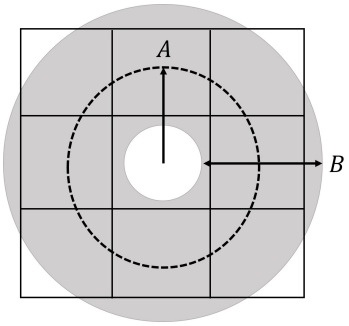

Figure 5.1: Range of neighbouring elements to include

In Figure 5.1 a simplification of a elements in a meshed grid is shown. Arrow 'A' resembles the radius and arrow 'B' the tolerance of neighbours to include when the element is under high stress. Values are typically one element size e_s. With this combination of radius and tolerance the neighbouring elements are selected.

5.2.2. Random Start
When the starting point of a TO is in a state where all elements are included, the overall average stress per element is extremely low. There will be a lot of elements with almost no stress and just a few that will be in a hot-spot where the load or the constraints are applied. This requires a tentative parameter setting where the RR is kept extremely low for a long time to prevent the removal of too much material, resulting in a large number of required iterations for a stable solution. A solution is to start the optimization in a state where element stresses are altogether higher, which means that the RR ratio can start more aggressively and therefore needs less iterations. One way to do this is to begin with a randomly generated layout as shown in Figure 5.2.

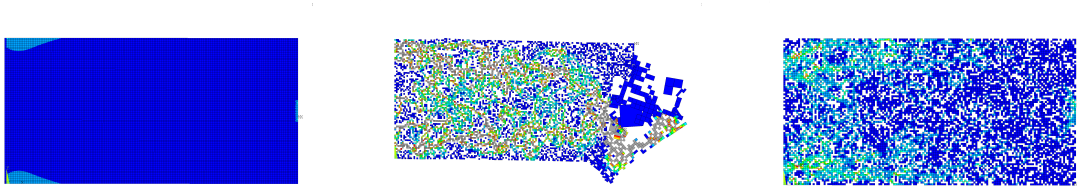

(a) (b) (c)

Figure 5.2: (a) fully included start, (b) [0.001,1] random start and (c) [0.001,1,1] random start

Figure 5.2(b) shows a sparsely filled starting condition which is unstable and has a high chance of resulting in a structure with an unreasonably high stress. A solution to this is to start with a structure that is filled for approximately two-thirds of the available volume. This is done by assigning each element with a value randomly chosen out of the vector $E_{start}[i] = [0.001, 1, 1]$. Now the structure has the tendency toward a more filled in starting volume and therefore a stable run.

Another advantage of this method is that every start has the possibility to have a different result. If the results generally have the same structure, it could be argued that this is close to the global optimum. In global optimization using a multi-start approach is a way to give more confidence to the solution and the same concept could be applied with MBESO. Next to that it can also act, to a degree, as a sensitivity analysis where different solutions give more insight in the problem. The proposed method is to have a total of four runs, one starting out as completely included and three randomly started.

The random start becomes more useful with the NIR as this helps extremely well to find a quick convergence. However, it must be noted that these results can be used as a supplement when making design decisions.

5.2.3. Absence of Volume Constraint

In most encountered literature about ESO/BESO methods, a volume constraint was applied. This however, feels contradictory because the goal of the optimization is to reduce the structure to a minimal volume. However, when the objective is to minimize compliance a volume constraint can be convinietn. In the MBESO there is no volume constraint, which means that the tuning of the parameters (RR,IR,NIR,$i_{constant}$) must be taken into consideration to have a stable simulation and a good result. These have to be acquired by experience, just as with the normal BESO method. [5]

5.2.4. Ratios

With the BESO method the RR increases and IR decreases when a state of equilibrium is achieved. To get to an equilibrium where no elements are included or rejected for at least one iteration, the problem must be simple. If there are a lot of elements and especially with a random start, such a state takes a lot of iterations to achieve. A fast way of approaching the problem without this conditional, is to find a good ratio for IR and NIR to be constant over all iterations and to increase it slowly as Equation 5.1 describes. Figure 5.3 shows how the ratios stay constant or change over the iterations.

$$\sigma_{reject-element}[i] = \begin{cases} \sigma_Y \cdot RR \cdot sin\left(\frac{\pi}{2} \cdot \frac{i}{i_{constant}}\right) & \text{if } i \leq i_{constant} \\ \sigma_Y \cdot RR & \text{if } i > i_{constant} \end{cases} \tag{5.1}$$

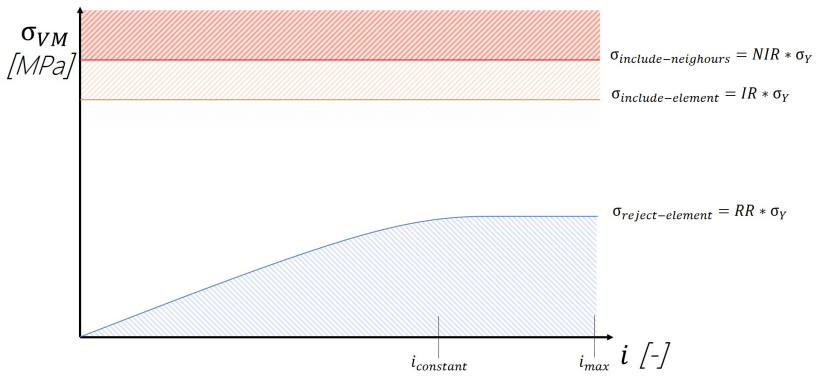

Figure 5.3: NIR, IR and RR visualized over number of iterations

5.2.5. Optimization Procedure

In every iteration, all the Von Mises stresses per element are checked. This is the basis for whether the element is rejected, included or if even its neighbours are included. Each element has its own stiffness E_e, which by default is the the same Young's modulus of steel. The elements are not completely 'killed' but are given an extremely low Young's modulus which renders them virtually not contributing to the overall stiffness. To overcome an oscilating behaviour a check for this is implemented after all the RR,IR and NIR operations are done.

$$
\begin{aligned}
&for \quad i \quad in \quad range(0, \quad n_{iterations}) \\
&\quad for \quad k \quad in \quad range(0, \quad n_{elements}) \\
&\qquad if \quad \sigma_{VM,e} \geq \sigma_{include-neighbours} \\
&\qquad\quad E_e[i,k] = 1 \cdot E_{steel} \\
&\qquad\quad E_{e,neighbours}[i,k] = 1 \cdot E_{steel} \\
&\qquad elseif \sigma_{VM,e} \geq \sigma_{include-element} \\
&\qquad\quad E_e[i,k] = 1 \cdot E_{steel} \\
&\qquad elseif \quad \sigma_{VM,e} \leq \sigma_{reject-element}[i] \\
&\qquad\quad E_e[i,k] = 0.0001 \cdot E_{steel} \\
&\qquad endif \\
&\qquad if \quad E_e[i-2,k] \neq E_e[i-1,k] \quad and \quad E_e[i-2,k] = E_e[i,k] \\
&\qquad\quad E_e[i,k] = E_e[i-1,k] \\
&\qquad endif \\
&\quad endfor \\
&endfor
\end{aligned}
$$

All these values are stored in a vector and passed on to the FEA to incorporate them and solve for this new structure. When the FEA has been executed and each element is in a new stress state, the process repeats itself.

Since the objective of this optimization is to minimize mass, the following objective function has been formulated. The number of included elements is multiplied with the element size and thickness and is subsequently multiplied with the density of steel to find the mass.

$$mass_{wf} = n_e \cdot e_s \cdot e_s \cdot t_{wf} \cdot 8050 \cdot 10^{-12} \quad [tonne] \tag{5.2}$$

5.2.6. Verification of MBESO

With these modifications applied, it is required to check whether the results of the altered method are logical and resemble existing results from literature. The main comparison that

will be made is between the resulting structures from the MBESO and TO literature. This can be satisfied with a visual check and the results do not have to match completely on elemental level as this data is not available. The benchmarks use PLANE182 elements that only work in the xy-plane, making it 2D models.

Neighbour Inclusion Ratio Effect with BESO Benchmark

Querin [21] used two benchmarks to test the method. For this simple geometry the algorithm will also get to the final result with solely removing elements. To overcome this, and to show the significance of the inclusion ratio, the experiments were set up in a starting point with the least amount of material required. That means that the location of the load introduction has to be connected to the kinematic constraints and nothing more. Two benchmarks were used; the 'two bar frame' and a 'Michell type'. The MBESO will also be subjected to these and a comparison will be made to find out whether the NIR has an effect on the result and amount of iterations.

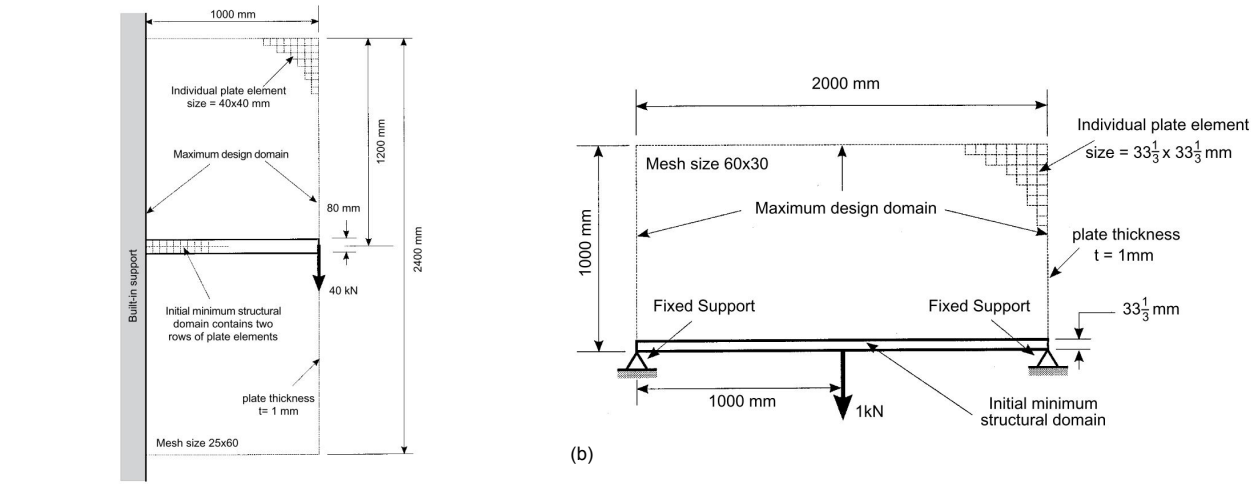

Figure 5.4: Two bar frame BESO Benchmark (a) and the Michell Type structure (b)[21]

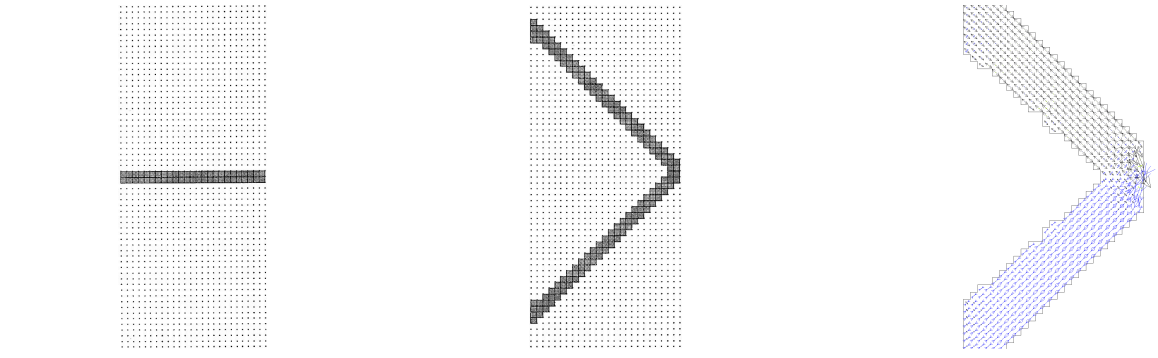

Figure 5.5: Two bar frame BESO Benchmark (a) setup, (b) starting condition [21] and (c) result where the blue vectors resemble compression and the black imply tension.

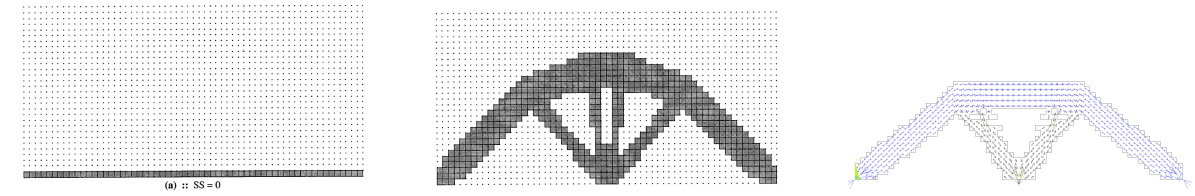

(a) (b) (c)

Figure 5.6: Michell type BESO Benchmark (a) setup, (b) starting condition [21] and (c) result where the blue vectors resemble compression and the black imply tension.

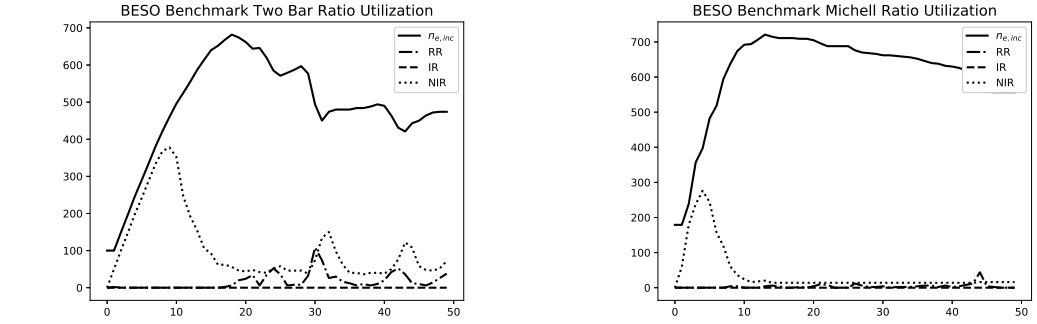

(a) (b)

Figure 5.7: Ratio utilization and number of included elements per iteration step

The similarities are striking between the benchmarks, albeit that the difference between the modified and the original method are that the original method continues to increase the RR with each steady state number. The modified method is a lot more crude in this instance as these parameters are tuned to find a similar solution. However, what is not mentioned in the papers is the maximum stress that is allowed to find these structures, what is known though is that the maximum stresses in these structures are extremely high. Far outreaching the normal yield stress of 235 [MPa] by being in the range of 10 times as much. So when it is applied to real life situations, as with the midsection the algorithm is able to push it beyond what is realistic. From these similar results it can be concluded that the main principles are reached, but to find the exact same structure is difficult and not realistic.

The BESO method would need 50 steady state solutions [21], but it is uncertain how many iterations each steady state takes. The MBESO was set to find this solution in 100 iterations. The neighbour inclusion will help the structure grow extremely fast at the start, but it might cause unwanted oscillation at the end when all the elements are fully stressed.

Cantilever Beam Benchmark

The geometry and loading are according the thesis by [15], who gathered a lot of TO researches and condensed them to general geometries. An often encountered problem in TO is the cantilever beam. It is clamped on the left side and a load is applied on the center right. The main dimensions and parameters for this optimization can be found in Table 5.1 and a visualization in Figure 5.8. The black triangles represent the structural constraints and refrain the nodes from moving in the direction of the triangle. This model constrained in vertical and horizontal direction over the complete left side, therefore also eliminating rotation of that line making it a clamped constraint. An expected outcome is shown in Figure 5.9.

item	value	unit
e_s	12.5	[mm]
P	300	[N]
L	160 e_s	[mm]
W	80 e_s	[mm]
RR	0.125	[-]
IR	0.65	[-]
NIR	0.70	[-]
$i_{constant}$	40	[-]
i_{max}	50	[-]

Table 5.1: Model parameters.

Figure 5.8: Cantilever beam loading and constraints.

Figure 5.9: Cantilever Beam expected outcome [15]

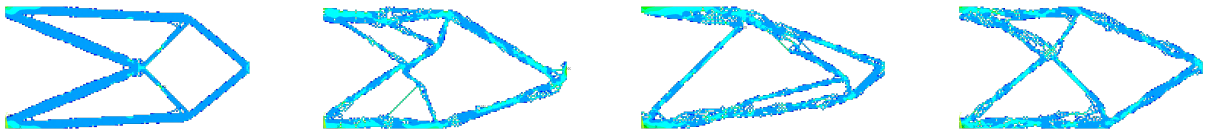

(a) (b) (c) (d)

Figure 5.10: (a) fully included start (b), (c) and (d) are random starts.

The fully included start (FIS) is comparable to the literature as found in Figure **??**.

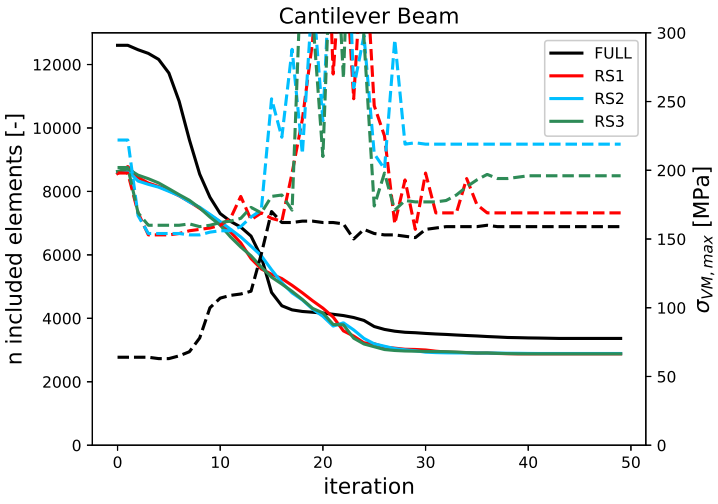

Figure 5.11: Full and random start comparison in number of elements and maximum Von Mises stress of cantilever beam benchmark.

result	$n_{elements}$ [−]	$\sigma_{VM,max}$ $[MPa]$
FULL	3366	158
RS1	2881	169
RS2	2891	218
RS3	2881	196

ratio	$\frac{n_{e,RS}}{n_{e,FULL}}$	$\frac{n_{e,RSx}}{n_{e,START}}$
FULL	1	0.263
RS1	0.856	0.225
RS2	0.858	0.225
RS3	0.856	0.225

Table 5.2: Final solution number of elements and maximal Von Mises stress for the cantilever beam benchmark.

Michell Benchmark

The Michell benchmark only uses simply supported constraints and therefore the geometry experiences a mostly evenly distributed stress, except on the point where the vertical constraints end. This makes it particularly difficult to optimize as the elements far away from the hot-spot do not necessarily have a high stress, but do have a significant effect on the magnitude of the hot-spot stress. If the beam that connects the top left with the bottom right has almost no radius, the direction of the stress tends more toward a horizontal direction. This creates a moment and therefore a lot of stress on that location, while the rest of the elements are well below the threshold to be included or include the neighbouring elements.

Therefore a more subtle approach is needed to have a less steep increment of the RR. The expected result is shown in Figure 5.13.

item	value	unit
e_s	10	[mm]
P	150	[N]
L	100 e_s	[mm]
W	100 e_s	[mm]
RR	0.075	[-]
IR	0.50	[-]
NIR	0.50	[-]
$i_{constant}$	70	[-]
i_{max}	80	[-]

Table 5.3: Model parameters.

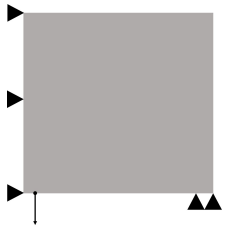

Figure 5.12: Michell type structure loading and constraints.

Figure 5.13: Michell benchmark expected outcome [15]

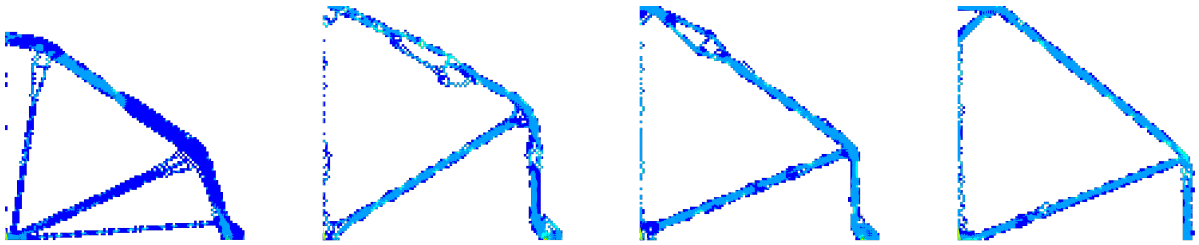

(a) (b) (c) (d)

Figure 5.14: (a) fully included start (b), (c) and (d) are random starts.

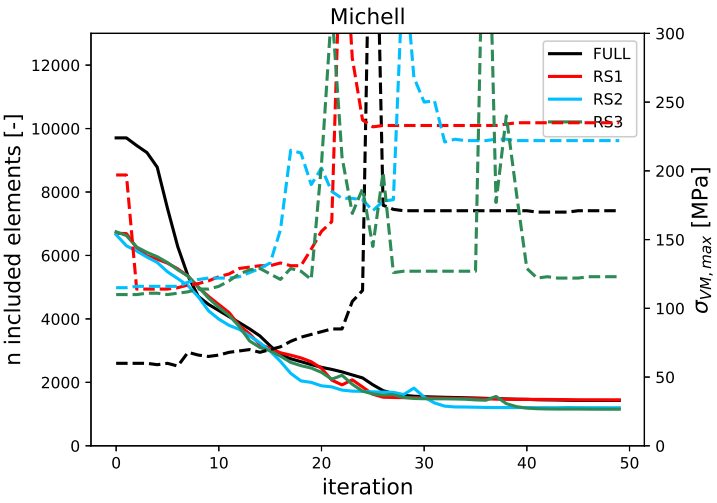

Figure 5.15: Full and random start comparison in number of elements and maximum Von Mises stress.

result	$n_{elements}$ [−]	$\sigma_{VM,max}$ [MPa]
FULL	1430	132
RS1	1199	222
RS2	1153	12
RS3	1163	180

ratio	$\frac{n_{e,RS}}{n_{e,FULL}}$	$\frac{n_{e,RSx}}{n_{e,START}}$
FULL	1	0.143
RS1	0.838	0.120
RS2	0.806	0.115
RS3	0.813	0.116

Table 5.4: Final solution number of elements and maximal Von Mises stress.

The vertical line next to the horizontal constraints is the result of residual stress that is still left in the elements that are virtually not there, but do still contribute a little bit.

L-Beam Benchmark

Another common benchmark is the L-beam. This has the property of creating a hot spot in the inside of the 'knee'. What is important is that the way the stress is relatively distributed

amongst the elements. This creates the same problem as found in with the Michell benchmark but the maximum amount of iterations can still be the usual 50. The result for the L-beam topology optimization is shown in Figure 5.17.

item	value	unit
e_s	10	[mm]
P	100	[N]
L	150 e_s	[mm]
W	60 e_s	[mm]
RR	0.05	[-]
IR	0.50	[-]
NIR	0.55	[-]
$i_{constant}$	40	[-]
i_{max}	50	[-]

Table 5.5: Model parameters.

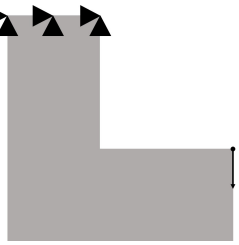

Figure 5.16: L-beam loading and constraints.

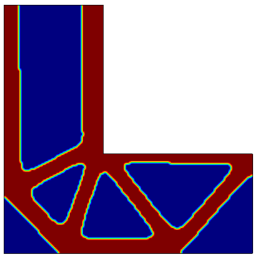

Figure 5.17: L-Beam expected outcome [15]

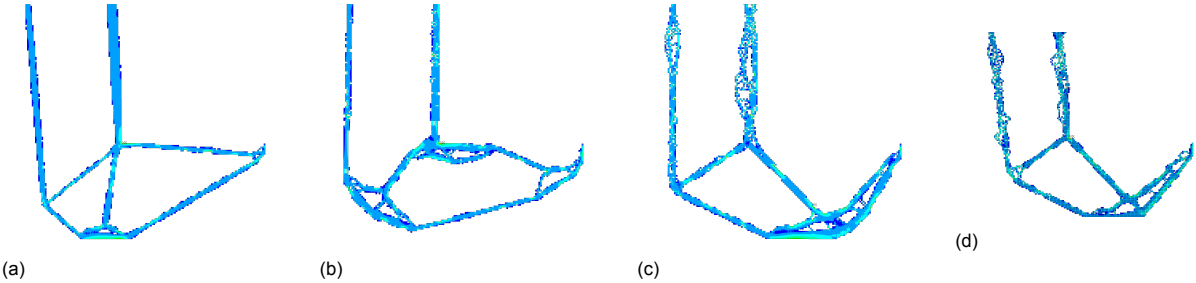

Figure 5.18: (a) fully included start (b), (c) and (d) are random starts.

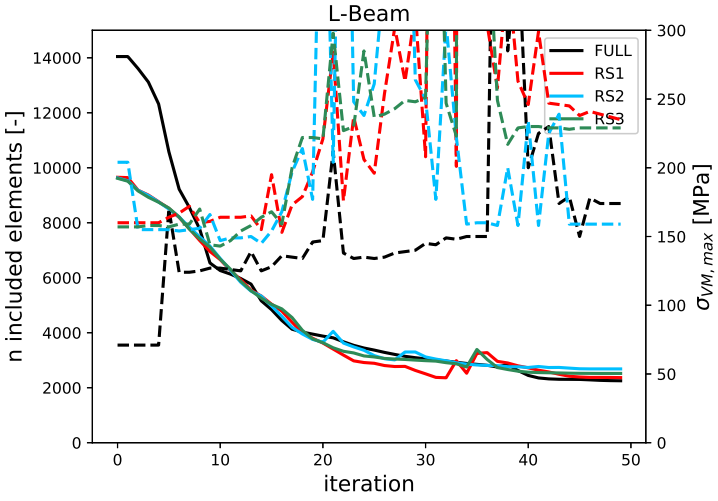

Figure 5.19: Full and random start comparison in number of elements and maximum Von Mises stress.

result	$n_{elements}$ [−]	$\sigma_{VM,max}$ $[MPa]$
FULL	4432	107
RS1	3517	134
RS2	3301	159
RS3	3700	201

ratio	$\frac{n_{e,RS}}{n_{e,FULL}}$	$\frac{n_{e,RSx}}{n_{e,START}}$
FULL	1	0.308
RS1	0.806	0.244
RS2	0.745	0.209
RS3	0.835	0.257

Table 5.6: Final solution number of elements and maximal Von Mises stress.

Benchmark Discussion

From the benchmarks it shows that this method is quick, can deal with unmapped meshes such as the L-beam and the random starts create the possibility to generate new structures that can be used as a sensitivity analysis or it could provide new design ideas. To sum up:

1. The benchmarks show an overall good resemblance to literature. For runs that start with all elements included, the general shape matches what could be expected. The random starts do show resemblance in the case of the Michell and L-beam, but are a porous version of it. With the cantilever beam the shapes differ more from each other, but that shows how the MBESO could be used; different options show the dependency of the structural members.
2. The amount of iterations required for the result is generally low.
3. A lot of other aspects of these models are interesting, to research the effect of the radius and tolerance of the NIR and a sensitivity study of the RR,IR and NIR but this was only done to verify the method.

5.3. Geometry

The geometry is almost the same as the numerical stiffened panel model, with the exception that the bilge in this geometry is rounded. The hull plates also do not have stiffeners attached to them, but will be of a thickness that was the result of the SO. So the longitudinal plates are not variable, but all the elements representing the web frame are and will be handled in the same manner as shown in the benchmarking of the MBESO method. The elements used in this optimization are SHELL181 and an element size of 100 [mm] was selected.

To have a minimal effect on the outcome, the constraints are placed on the outer sides which would be halfway between the frames. At that position, the rotation around the z and x axis should be equal to zero. The orange double arrows resemble the rotational constraint.

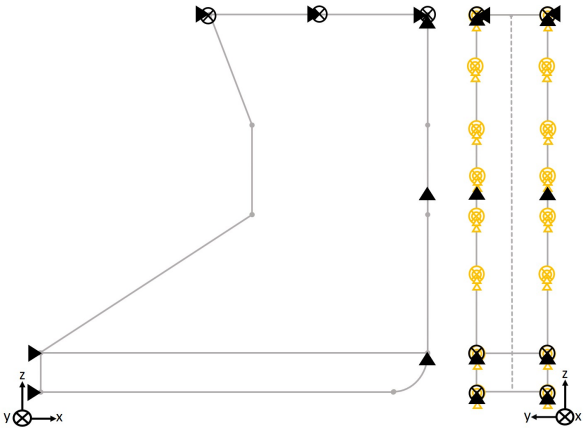

Figure 5.20: Web frame numerical model constraints.

5.4. Loading

The loading is simulated as if the midsection were in the hogging condition and fully loaded. That way, the most amount of pressure is put into the structure. There is only local loading induced by hopper load and water pressure. The global load is regarded to be entirely absorbed by the longitudinal stiffeners.

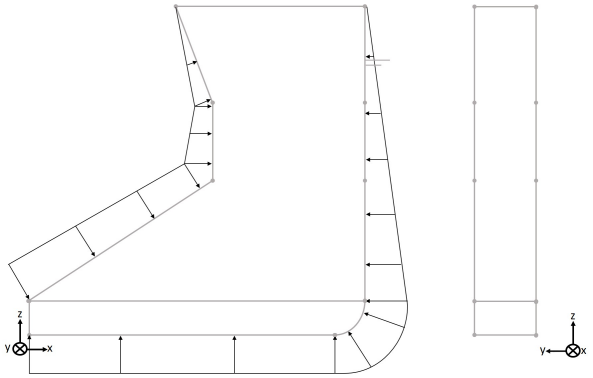

Figure 5.21: Web frame loading in maximum hogging condition for maximum load.

5.5. Optimization Parameter Setting

To keep the optimization a quick tool, the maximum amount of iterations is chosen to be 50. This determines the rest as a longer optimization with a more delicate ratio setting might also be a good option. Next to that it also determines the

item	value	unit
e_s	100	[mm]
RR	0.125	[-]
IR	0.65	[-]
NIR	0.70	[-]
$i_{constant}$	40	[-]
i_{max}	50	[-]

Table 5.7: Model parameters for the web frame topology optimization.

5.6. Web Frame Thickness

In the reference ship the web frame is a large T-stiffener that is mainly constructed with webs of 700 and 1050 [mm], but a constant thickness of 12 [mm] and a flange of 150x12 [mm]. To stay in the same order of dimensions, the web frame thickness for the TO should be more than 12 [mm] to compensate for the flange. If the thickness is too large, the optimization parameters should be changed. A sensitivity study has been done for 4 different thicknesses: [12, 15, 18, 21] [mm]. These are based on the area and moments of inertia shown in Table 5.8

$h_w[mm]$	T	I	$t_{wf,12}$	$t_{wf,15}$	$t_{wf,18}$	$t_{wf,21}$
$A_{700}[mm^2]$	10200	12000	8400	10500	12600	14700
$I_{700}[mm^4]$	$5.07 \cdot 1e8$	$7.35 \cdot 1e8$	$3.43 \cdot 1e8$	$4.29 \cdot 1e8$	$5.15 \cdot 1e8$	$6.00 \cdot 1e8$
$A_{1050}[mm^2]$	14400	16200	12600	15750	18900	22050
$I_{1050}[mm^4]$	$1.55 \cdot 1e9$	$2.05 \cdot 1e9$	$1.16 \cdot 1e9$	$1.45 \cdot 1e9$	$1.74 \cdot 1e9$	$2.03 \cdot 1e9$

Table 5.8: Equivalent web frame plate thickness in comparison to T and I beams

For a load that causes a moment, the moment of inertia is important. For membrane stress however, the area is the dominating structural property of a beam. The comparison in Table 5.8 is made for both a T-stiffener and and I-beam, resembling an equivalent flat bar when the TO connects material alongside the hull plates and an equivalent beam when only connected to the hull on either end.

The plate thicknesses of all the hull plating is set to 20 [mm] to ensure that it is equally distributed and does not take up an unreasonable amount of stress and the WFS was taken

at 2250 [mm].

The least chaotic topology is the one with 18 [mm] as can be seen in Appendix B Figure B.3 and it has a comparable equivalent moment of inertia and area of a web frame T-stiffener with the dimensions of [1050x12,150x12]. These are the minimum dimensions found in the reference web frames, but thicker webs were found as well so the choice of 18 [mm] for the web frame thickness is in the same order of magnitude.

5.7. Underlying Mechanisms

To be able to understand the mechanisms that influence the final result a couple of smaller models are created. Especially the bottom of the hopper will be an area of interest as this is where the most of the load is concentrated. At first five different beams will undergo a topology optimization to find out how the optimizer deals with shear forces, this is followed with basic models that are derived from the main geometry. From the paper by Tschullick [22] it can be seen that beams are created. To see why this is the case, the bottom of the hopper tank and a double bottom are created and loaded with the hydrostatic pressure from the hopper contents, the water pressure and the combination. These models were created with PLANE182 elements, the hydrostatic loads were the same as described in Table 4.1 and the element size is 100 [mm].

5.7.1. Aspect Ratio Analysis

To find out whether the optimization actually follows natural shapes an aspect ratio analysis has been done. The natural phenomenon to be found is that shear stress is distributed along 45 degrees through the isotropic material. Five models were created with each a different aspect ratio. The bottom half of the shapes are filled for the starting condition in order for the inclusion ratios to also have effect.

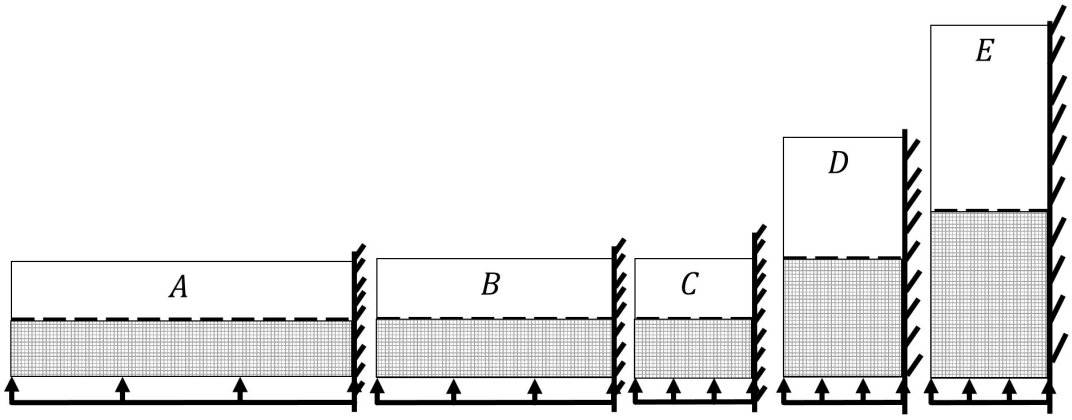

Figure 5.22: Aspect Ratio Models

models	A	B	C	D	E
vertical n_e	50	50	50	100	150
horizontal n_e	150	100	50	50	50
total n_e	7500	5000	2500	5000	7500

Table 5.9: Design space specification for each aspect ratio model

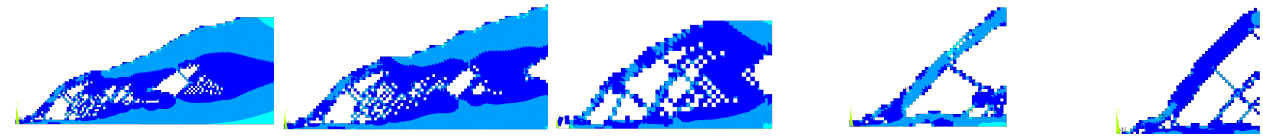

(a) (b) (c) (d) (e)

Figure 5.23: Results of different aspect ratios, unscaled for better visuality. Relative size can be derived from Figure 5.22 and Table 5.9

The results for model A and B show that the top elements are filled to overcome with the moment due to the large span. However, when the beam is shorter a lot less material is needed to withstand the loads. While the 'tip' of the structure shows a beam under a rough 45 degree angle in models A,B and C, the results for D and E do show a clean beam under the expected angle and therefore geared for shear. The expected outcome of model C, D and E is to be completely the same as the design domains have the same width and are under the same load. This is, however, where the MBESO's crude nature is shown. A more refined method would have given the same result for the C, D and E models.

5.7.2. Reduced Models

To better understand the final results, parts of the structure were created to find their contribution to the final result. A total of four basic models were created and can be found in Appendix C, but the two most important are shown here. The Von Mises stresses lack the ability to find out whether a beam is in tension or in compression, the following results are depicted with the vectors for the first and third principal stress. All the elements in tension will have the first principal stress as dominant stress and consist out of black vectors, whereas the elements in compression will show blue vectors meaning that the third principal stress is the largest.

Bottom Hopper and Double Bottom

The results show that when only one pressure is applied a large moment is induced that has to guide the stresses to the kinematic constraints. However, when both the pressures are applied, the load can be diverted to each other, resulting in beams between the loads and the orientation in the direction of the higher load.

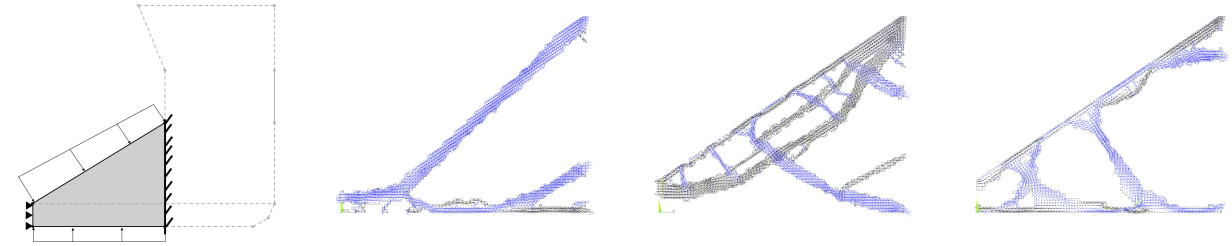

(a) (b) (c) (d)

Figure 5.24: Bottom of hopper tank with double bottom fundamental model with (a) water pressure, (b) hopper pressure and (c) water and hopper pressure combined

A similarity with the aspect ratio is demonstrated in Figure 5.24(b). In essence, these are the same and the MBESO creates a beam of approximately 45 degrees to be most efficient of taking up the shear that is induced by the vertical water pressure and has to be transferred to the kinematic constraints.

Another remarkable finding is that when both the hopper and water pressure are applied, less material is needed. This happens because the total moment that the constraints have

to take in is reduced as the moments by both pressures are in opposite direction. That way, the stresses can be conveyed to the opposing load and no material is needed for the extra moment and to transport the load to the constraints.

Bottom Hopper, Double Bottom and Side Geometry

This geometry is the same as the previous one, but now the kinematic constraints are further away from the load introductions, creating a larger moment.

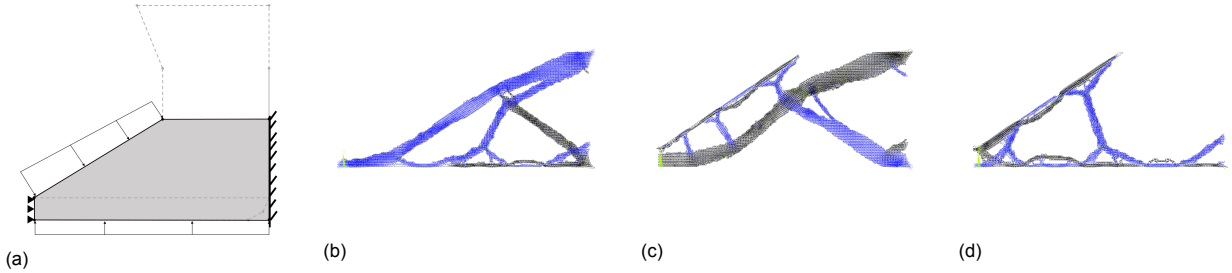

Figure 5.25: Bottom of hopper tank with double bottom and side compartment fundamental model with (a) water pressure, (b) hopper pressure and (c) water and hopper pressure combined

The same principles apply as previously mentioned, but because this model is closer to the actual geometry, the combined hopper and water pressure result are of interest. In the bottom right corner of Figure 5.25(b) and (c) a similarity is shown that is also reoccurring in the aspect ratio. This is where shear is guided into the side shell of the ship.

5.8. Results

Per web frame spacing a total of eight results were produced. Four of these were with an unscaled web frame thickness of 18 [mm], consisting of one fully included start and three random starts. The other four have a scaled web frame thickness and one fully included start and three random starts as well. A complete overview of the results can be found in Appendix D, but the best ones selected from the complete set are depicted here.

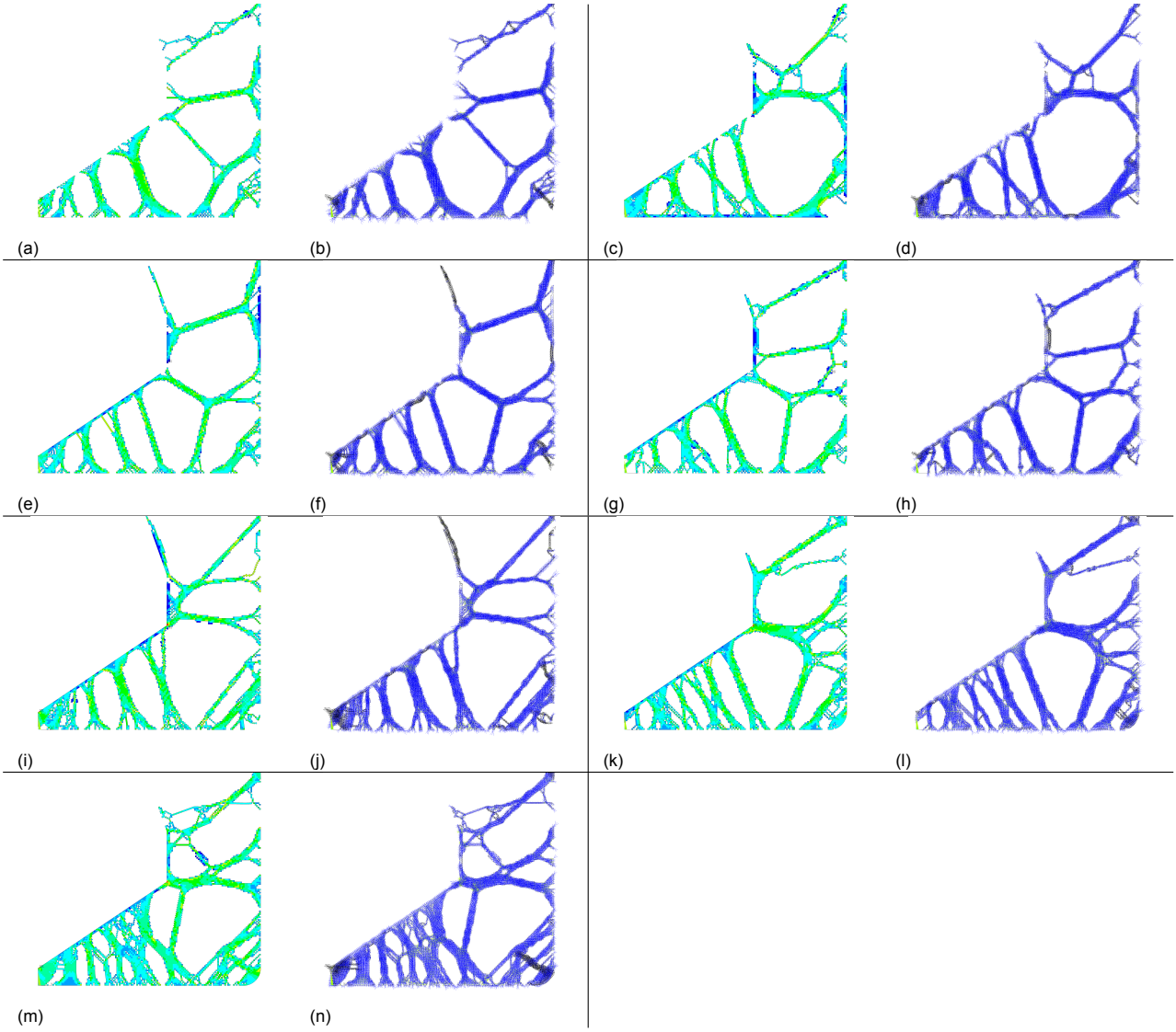

Figure 5.26: Topology optimization results of WFS = (a) 562.5 [mm] (b) 1125 [mm] (c) 1687.5 [mm] (d) 2250 [mm] (e) 2812.5 [mm] (f) 3375 [mm] (g) 3937.5 [mm]

To get a good approximation of the mass, the number of elements is multiplied with the element size, the element thickness and the density of steel. Because a mapped mesh was not possible, it can only be an approximation.

WFS [mm]	562.5	1125	1687.5	2250	2812.5	3375	3937.5
$n_{e,inc}$	3075	4985	4906	4858	6222	6616	7507
t_{wf} [mm]	4.5	9	13.5	18	18	18	18
mass [t]	1.11	3.61	5.33	7.04	9.02	9.59	10.88
$\sigma_{VM,max}$ [MPa]	174	211	173	168	231	226	232
start cond.	RS	RS	RS	RS	RS	RS	RS

Table 5.10: Best selected solutions from topology optimization

5.9. Discussion

5.9.1. Common Beams

To help the discussion on common beams, Figure 5.27 was created.

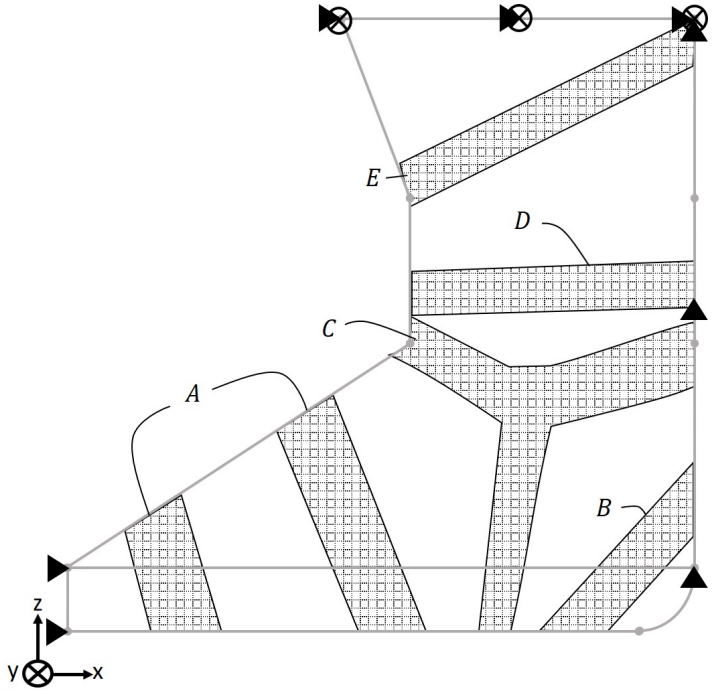

Figure 5.27: A sketch of common beams in the final TO results

A
The most common beams are these, in the sketch only two beams are drawn but these vary in number. The orientation of these however, are mostly the same and the orientation is in the direction of the hopper load. From the fundamental models it was learned that these help to relieve the kinematic constraints by transferring both of the loads toward each other to diminish their effect. These are in pure axial stress.

B
This beam resembles the shear transfer from the upward hydrostatic pressure. Not only does it face the hydrostatic pressure from the side shell, but it also prevents vertical displacement through the kinematic constraints.

C
This is the most complicated beam as it solves various stress paths. The corner in the hopper where the inclined bottom of the tank has a transition to the vertical part is a common problem for stress concentrations. This concentration of stress is leaning on the hydrostatic pressure and its horizontal part has to be taken in by the horizontal water pressure.

D
In most solutions this horizontal beam helps the inward deflection of the vertical part of the hopper and the center panel of the side shell.

E
In some solutions such as seen in Appendix D Figure D.2(e) and (f) this beam is not present and that results in a stress concentration at the location where the tank top connects with the bottom inclined panel of the hopper tank. If the pressure in the hopper tank is not diverted to the hydrostatic pressure, the vertical and horizontal kinematic constraints in the outer corner of the main deck, it will create a moment around the y-axis and therefore a stress concentration at the lowest part of the hopper tank.

5.9.2. Neighbour Inclusion Ratio with Random Start

To see the effect of the ratios in a random start, Figure 5.28 shows the utilization of each ratio over the iterations.

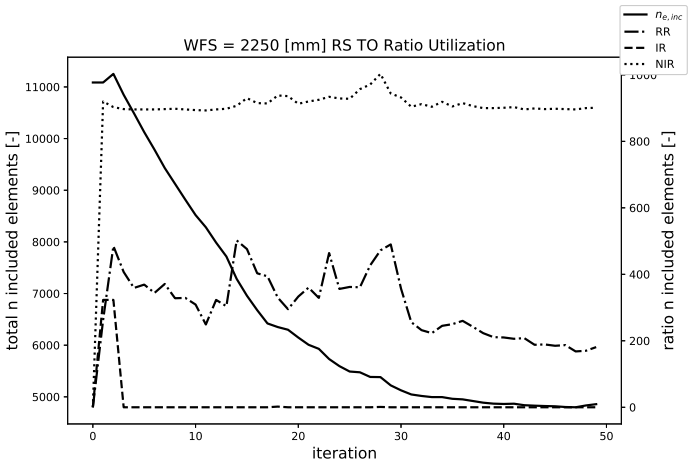

Figure 5.28: Ratio utilization of the result in Figure 5.26(g) and (h). Please note that the left y-axis is for the total number of elements and the right y-axis is for the ratios.

The most dominant ratio over the optimization is the NIR, but it must be kept in mind that this analysis also counts elements that are already included. The IR shows a small contribution in the beginning because with a random start it is much easier to overcome the threshold of including a single element, however when the geometry start to take shape the probability of an element being in a stress state lower than the NIR but higher than IR is low.

5.9.3. Deflection

To even better understand the results, a supplementary deflection plot was created. It is evident that the water pressure is dominant as the mid of the hopper is pushed upward. This is due to the fact that the loading condition was set as if a wave travelled past the section.

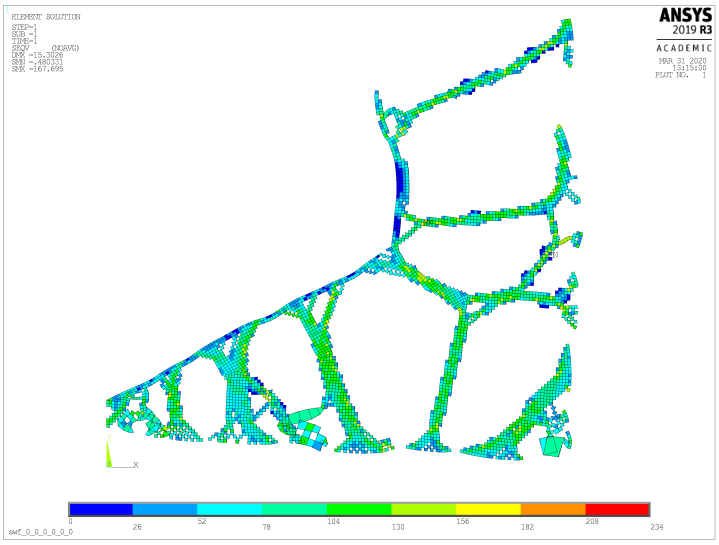

Figure 5.29: Stress plot with deflection.

5.9.4. Random Start

There are a lot of differences between the solutions, but that can help understand the problem. As Figure D.4(b) and (c) show that an absence of an inclined beam to the top of the hopper will result in a high stress where the ship would be mirrored between the keel plate and the tank top.

The similarities however, display what can be learned from this optimization. A striking contrast with the conventional way of constructing a web frame along the hull plates, is that beams are created that have a perpendicular instead of a parallel orientation toward the hull plating. This makes sense, as the least amount of material is used when a structure is in membrane stress where the stress distribution throughout is constant. A beam that is loaded with a moment, has a neutral axis which does not endure any stress and thus rendering it a less efficient use of material. This understanding will help the designer in the next step of making the structure ready for production and determining the compartments.

5.9.5. Limitation

A limitation of these results is that it optimizes the model and not necessarily the real life situation. At the moment the outer vertical hull plating is constrained in vertical direction, modelling how the ships buoyancy and weight distribution are kept in balance. The hopper tank contains more weight than that the specific geometry can provide in buoyancy, so the rest of the ship will be used to find an equilibrium. This stress is mostly conveyed through all vertical plates and not only the outer vertical shell. So the optimization can improve the understanding of the ship structure, but it cannot directly be implemented in the final design due to the fact that there is a discontinuity between the model and the real life situation.

5.9.6. MBESO Coarseness

From all the optimization methods, the element based optimization such as SIMP and BESO are not the most refined ones. On top of that, the MBESO is even less refined as it does not wait for a status quo before altering the ratios as the normal BESO would. So even more refinement is traded for quick convergence of large problems with unmapped meshes.

5.9.7. Design Tool

Finally, these results can help start the discussion as to how to implement the web frame. It is obvious that these organic shapes are hard to manufacture, but it could support design decisions of how to orient the beams and how to divide the compartments for an optimal strength.

6
Optimization Interaction

6.1. Introduction

The optimization procedure dictates that the SO should be performed before the TO as this is used as input. The thicknesses and therefore the stiffness of the panels are variable, but in what way do these changes have an effect on the topology outcome?

In this chapter the reference WFS will be used and three different situations will be discussed. As all the panels have an effect on each other, the ones that are most straightforward for this mechanism are the side hull plates. It would be interesting to see whether the TO reinforces the weaker parts or support the stiffer neighbouring panels.

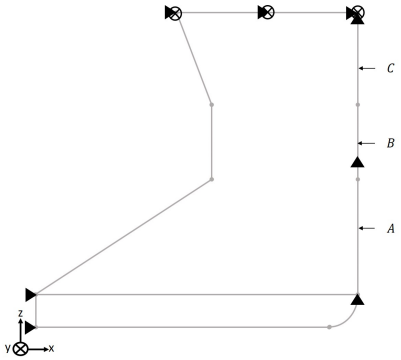

Figure 6.1: All surrounding plates of 24 [mm] except A-(bottom shell), B-(mid shell) and C-(top shell) of 4 [mm]

6.2. Results

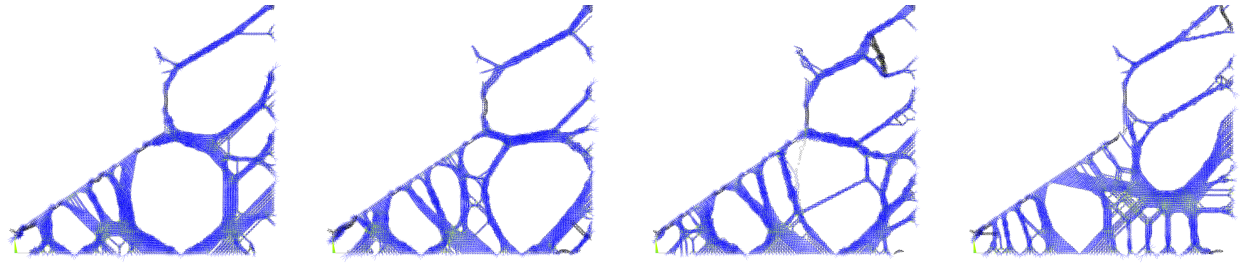

(a) (b) (c) (d)

Figure 6.2: All surrounding plates of 24 [mm] except (b) panel thickness of A = 4[mm] (c) panel thickness of B= 4[mm] (d) panel thickness of C = 4[mm]

6.3. Discussion

The results show how the shear of the vertical water pressure is transferred to the side hull. In Figure 6.2(d) a lot of material is needed in the lower region as most of the vertical stress cannot be taken up with the top part of the shell, but a moment is created as it needs to be transferred to the bottom hopper. So two mechanisms are identified, if a plate with a high hydrostatic pressure is thin, the web frame would support it with more material to prevent a

high amount of deflection. However, if the hydrostatic pressure was low and the plate is thin, the web frame is not able to transfer shear into that plate and therefore had to create more material elsewhere to support the vertical hydrostatic pressure. These mechanisms confirm the interaction between the shape optimization and the topology optimization.

7 Optimal Web Frame Spacing

Seven different options have been calculated for different web frame spacings. There might be an optimum between a lot of small web frames and a lighter longitudinal layout or a large spacing that is more heavily stiffened. To be able to compare these all total weights are divided by its respective WFS, resulting in a tonnage per meter. The lightest solutions that do not exceed the maximum Von Mises stress of 235 [MPa] are combined to find the total weight of a part of the midsection and are gathered in Table 7.1.

WFS [mm]	562.5	1125	1687.5	2250	2812.5	3375	3937.5
$mass_{ps}$ [t]	5.62	11.05	17.73	26.03	32.64	40.56	59.02
$mass_{wf}$ [t]	1.11	3.61	5.33	7.04	9.02	9.59	10.88
$mass_{tot}$ [t]	6.73	14.66	23.06	33.07	41.66	50.15	69.90
$mass_{tot}/WFS$ [t/m]	12.79	13.03	13.67	14.70	14.81	14.86	17.75

Table 7.1: Lightest combination per web fame spacing

Table 7.1 shows the best option to be smallest web frame spacing and the web frame with a scaled thickness. However, the stiffened panel relies on an infinitely stiff web frame and the web frame is the least stiff in this situation. With a larger WFS this effect diminishes, but will still be present. Keeping this in mind, the second contender is the WFS of 2250 [mm].

7.1. Midsection Comparison

To see how the optimized structure relates itself to the reference ship, both are displayed in Figure 7.1 and Figure 7.2 respectively.

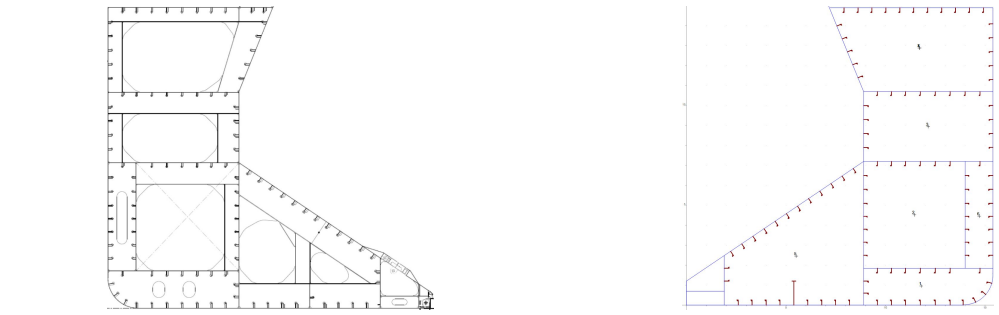

(a) (b)

Figure 7.1: Web frame and longitudinal stiffener arrangement of reference ship.

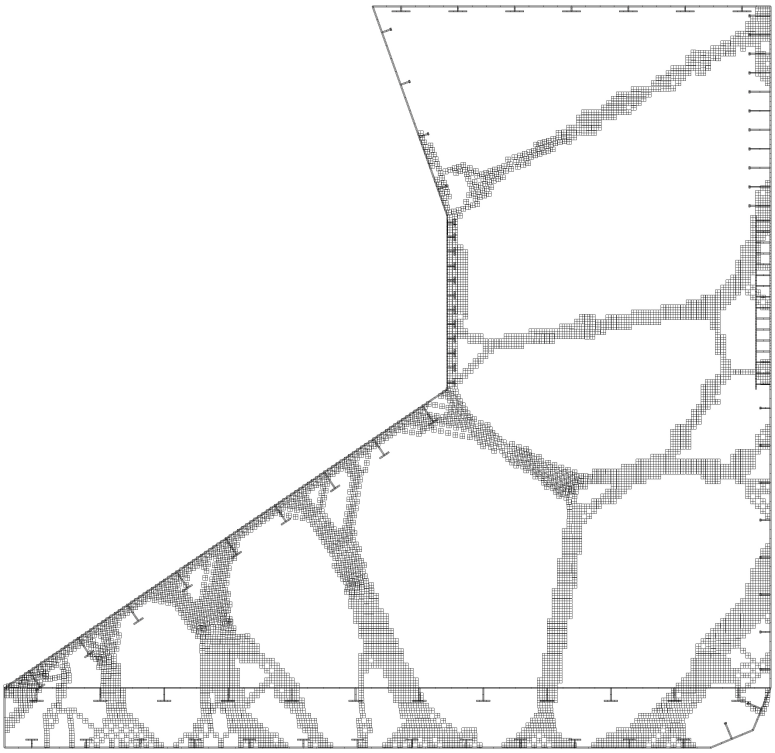

Figure 7.2: Web frame and longitudinal stiffener arrangement of the optimized ship midsection.

Although the reference ship is already a fully designed shape with the distribution of compartments, a weight comparison is helpful to give an idea how the optimized result compares to the original midsection. Another difference is the simplification of the models, where internal decks and vertical plates are not included.

WFS [mm]	reference ship	optimized structure	weight improvement
$mass_{ps}$ [t]	34.22	26.03	24%
$mass_{wf}$ [t]	8.70	7.04	19%
$mass_{tot}$ [t]	42.92	33.07	23 %
$mass_{tot}/WFS$ [t/m]	19.07	14.70	23 %

Table 7.2: Weight comparison and percent improvement

7.2. Abstraction Procedure

Since the topology optimization results in organic beams that consist out of elements and therefore have rugged edges, it will be harder, if not impossible to produce. To overcome this, an abstraction process was made in Rhino, that fits a surface over the elements and adds a flange to the free edges to prevent buckling. A proposed abstracted final result would look like:

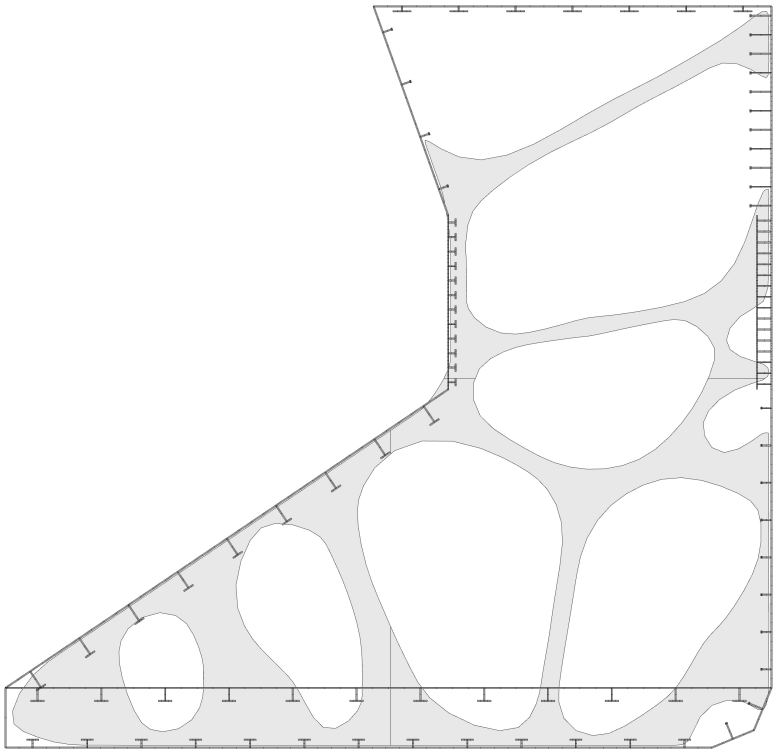

Figure 7.3: Abstraction of web frame and longitudinal stiffener arrangement of the optimized ship midsection.

7.3. Discussion

While the lightest solution per meter is the for the smallest web frame spacing, this model also copes with the most undesired model interference. The kinematic displacement constraints in the middle of the model represent an infinitely stiff web frame and when the span is small, the interaction becomes more significant and therefore leads to less reliable analysis. On top of that for most panels, the orientation of the plates for the analytical buckling analysis has changed. Whereas the long side is along the web frame and not along the stiffeners anymore. Because these effects continue, the choice was made to stick to the reference web frame spacing for comparison.

The 23% weight improvement is only a rough estimate with regard to what the final producable midsection would look like. The weight improvement is likely to decrease significantly after a few design iterations and before it is able to be manufactured and pass a classification check but it is most certainly an interesting start and could lead to new discussions early in the design phase of how to arrange the midsection construction.

III

Conclusions and Recommendations

8 Conclusion

In this research two models were created, an analytical shape optimization model and a topology optimization. With the analytical shape optimization model, a good solution for the layout of the longitudinal stiffeners in the midsection of a ship was obtained in relatively short time, which then undergoes numerical check. The best solutions were selected to find a matching web frame by means of a topology optimization. Two different topology optimizations were executed; one with a scaled thickness of the web frame and a constant one. The complete optimization procedure was performed a total of seven times, representing different designs with distinct web frame spacings that were based on the reference ship. This resulted in an optimum arrangement of longitudinal stiffeners, a matching web frame and the lightest form of a web frame spacing.

1. *How can the longitudinal stiffener layout of a ship midsection be optimized?*
   For optimization of the longitudinal strength, an analytical model was created that was driven by a Simulated Annealing optimization algorithm to find a good solution. The SA was selected as the optimization problem is a discrete one and this global optimization algorithm is capable of dealing with discrete variables.

   The stiffened panels were parameterized in a way that the plate thicknesses, amount of stiffeners and stiffener dimensions are variable. These SOV are then randomly generated to describe the structure and an FEA was run to calculate stresses and buckling factors.

   The variables for the optimization were the amount of stiffeners, their dimensions and the plate thickness. The optimization model run with these variables resulted in a mass optimized layout that could still withstand the water and hopper pressure combined with the global hull bending moment in sagging and hogging condition, without yielding and without violating a linear buckling constraint.

2. *How to optimize the transverse web frame of a ship?*
   Once the longitudinal layout has been determined, the transverse web frames were optimized. This was done via a topology optimization based on the BESO method. To speed up the process and since this is a large problem, some alterations have been made to the BESO method to make the procedure less delicate but still quick and accurate enough. The MBESO went through several benchmarks to compare it with conventional optimization methods. Several sub models were created that each highlighted important sections of the geometry to be able to interpret the results for the full geometry. The final optimization procedure resulted in a different way of orienting beams as web frames.

3. *What is the interaction between shape optimization and topology optimization?*
   To find a relevant thickness for the web frame panel, a study has been done with different panel thicknesses. A model was created where all the hull plating had a thickness of 24 [mm] except for one plate that would have a thickness of 4 [mm]. This would help understand how the topology optimization is affected by the shape optimization. Two mechanisms were identified, if a plate with a high hydrostatic pressure was thin, the web frame would support it with more material. However, if the hydrostatic pressure was low, the web frame was not able to transfer shear into that plate and therefore had

to create more material elsewhere to support the vertical hydrostatic pressure. These mechanisms confirm the interaction between the shape optimization and the topology optimization.

4. *What is the optimal web frame spacing for an optimized web frame topology combined with an optimal longitudinal stiffener layout for a given length of a midsection?*
Seven options of web frame spacing were analyzed to find the an optimal arrangement. With a short WFS, the span was smaller, resulting in a lighter longitudinal arrangement and web frame but it would have to be repeated more often. A point of discussion is that with a smaller web frame spacing, the infinitely stiff modelled web frame in the shape optimization plays a greater role as opposed to a larger WFS. In comparison to the reference ship, a total mass reduction of 23 % was established.

5. *How can optimization techniques be used for a better understanding of ship structures?*
In the early design stage, especially the topology optimization results can help open the discussion and let the computer do a virtual brainstorm. Especially the topology optimization of the web frame has shown how the stress paths move through the structure. The TO results showed that constructing beams not in an orthogonal way and along the ship hull but rather under various angles could reduce the total mass of the web frame. This can help in a later stadium of the design to make choices on how to subdivide the compartments.

This research has shown that a better understanding of a structure and its reciprocal mechanisms can be acquired through optimization. The most applied method at the start of designing a ship is to find ships that have comparable traits and use that as a beginning. Over the years, this copying of previous work has deterred creative thinking about the structures and the possibility of radical new solutions. By letting the algorithm find out a structure, this could be a better starting point for the complete design.

Limitations of this research are that all the solutions that were created do not consider the compartments and productivity. On top of that, the modified BESO method proved to be a crude analysis.

9 Recommendations

For continued research, the following subjects are advised:

1. To overcome the issue of optimizing the longitudinal stiffened panels with an infinitely stiff web frame, a coupled model could be created. This would be a computationally intensive exercise as for every distinct layout, at least 50 topology optimization iterations are needed. This would, however give an ever better model.
2. At the moment only the thicknesses of the plates for each panel are taken into account for the topology optimization. However, a more realistic representation would be to smear the stiffeners into the plate, resulting in a plate with orthotropic Youg's Moduli.
3. The g_1 used in the analytical optimization has proven to be too conservative. One way of solving this is to give the constraint more relaxation and another is to alter the method used to find the maximum stress. Right now it is modeled as a beam that is only simply supported on two sides but it would be an improvement to model it as a plate that is simply supported on three, and is free on one side.
4. When fatigue is implemented in the constraints, it would make the model even more complete.
5. The longitudinal stiffeners could also be swapped for different stiffeners like the Holland Profile. An even more practical solution would be that the optimization algorithm does not change the geometry of the stiffeners, but has access to a library of of options with pre-defined stiffeners that are already off-the-shelf available for the shipyard.
6. Another option to make the tool more practical is to use constraints set by classification bureaus like BV. When these constraints are applied, even less post processing of the outcome is needed to get it through the classification procedure.
7. Instead of having a minimum and maximum amount of stiffeners, a better way to approach the situation is to have a minium and maximum stiffener spacing. In the stiffened panel model now a plate from 5 meters has the same range of allowed stiffeners as a plate from 10 meter.
8. The random start topology optimization procedure could also be used by creating a significant amount of data and 'morph' these results together to see whether a new topology is created.
9. Make sure at least 3 elements are in the web for the plate stiffener model as this ensures a better analysis for the shear and buckling of this part.
10. A multiprocessor brute force version of the shape optimization might be able to calculate all the different longitudinal stiffener arrangement possibilities analytically in a overseeable timeframe. That way, the optimum can be established with a hundred percent certainty.

IV

Appendix and Bibliography

A

Direct Numerical Optimization Results

In this research an analytical approach was taken to calculate a lot of different options for the plate stiffener arrangement in a fast way. However, not all of the solutions were accepted after a numerical procedure. To overcome this, another approach was tried to skip the analytical calculations and directly do the numerical assessment. The drawback of this is calculation time because this takes a longer time to analyze and is dependent on the web frame spacing as a larger spacing means more elements and therefore an even more calculation expensive. This resulted in a thousand iterations and took up around the same time of approximately 14 hours. The problem with this is that he amount of iterations stand in no comparison to the possible amount of solutions of 365,615,000.

A.1. Simulated Annealing

Efficiency and computing time are important factors in this model. Each FEM calculation takes the most time compared to the creation of SOV and its fitness check. Therefore the SA is a the best choice of algorithm as it can judge whether the new SOV is accepted or not before checking the constraints. Once the calculation is done, it would be senseless to disregard the results hence these are still stored as design points. Albeit not a feasible design.

A schematic overview is shown below, where the F(x) is the fitness test and FEA(x) the finite element analysis from which the yield criterion and buckling factor are retrieved.

$$
\begin{aligned}
C &= x_{random} \\
F_{current} &= F(C) \\
G_{current} &= FEA(C) \\
&for \quad T \quad in \quad range(T_{max}, \quad T_{min}, \quad n_{iterations}) \\
&\quad N = x_{random} \\
&\quad F_{new} = F(N) \\
&\quad \Delta F = F_{current} - F_{new} \\
&\quad if \quad (\Delta F > 0) \\
&\quad\quad G_{current} = FEA(N) \\
&\quad\quad F_{current} = F_{new} \\
&\quad\quad C = N \\
&\quad elseif \quad \left(e^{\frac{\Delta F}{T}} > random(0,1)\right) \\
&\quad\quad G_{current} = FEA(N) \\
&\quad\quad F_{current} = F_{new} \\
&\quad\quad C = N \\
&\quad else \\
&\quad\quad C = C \\
&\quad if \quad \sigma_{VM,max} \geq 235 \quad or \quad BF_{min} \leq 2.5 \\
&\quad\quad F_{new} = false \\
&\quad endif \\
&endfor
\end{aligned}
$$

This is not the conventional way of applying the SA, but because it is not certain that the last SOV will be the best. Furthermore, SHELL181 elements are used with an element size of 150 [mm].

A.2. Result

Since this takes up a lot of time, only the reference web frame spacing of 2250 [mm] was calculated in this manner. The results are shown in Table A.1.

WFS [mm]	2250 5
mass [t]	26.23
$\sigma_{VM,max,sag}$[MPa]	60.48
$\sigma_{VM,max,hog}$ [MPa]	98.49
BF_{sag} [-]	10.96
BF_{hog} [-]	9.99

Table A.1: Mass, maximum Von Mises stress and buckling factor of the direct numerical optimization

The result is close to that of the analytical optimization method, which resulted in a mass of 26.23 [tonne].

A.3. Discussion

As the mass of the direct numerical optimization is higher than from the analytical one (26.03 [tonne]), this optimization is regarded as inferior. On top of that the time that it takes to create these results is dependent on the web frame spacing as more elements are required to analyze a larger web frame. On top of that the approval rate by the constraints diminishes as the web frame spacing is increased.

B
Appropriate Web Frame Thickness Analysis

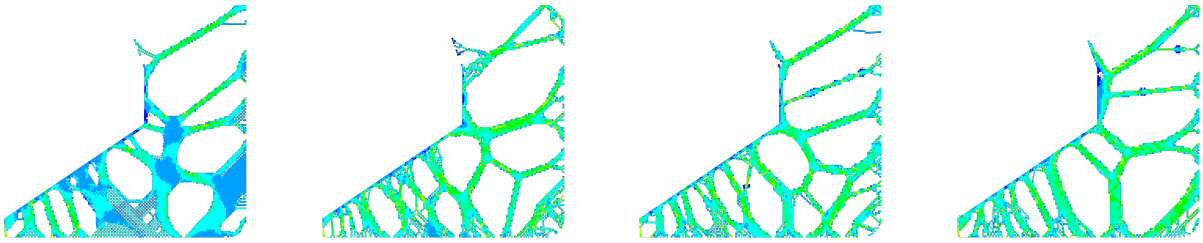

(a) (b) (c) (d)

Figure B.1: Web frame thickness of 12 [mm] (a) fully included start (b), (c) and (d) are random starts.

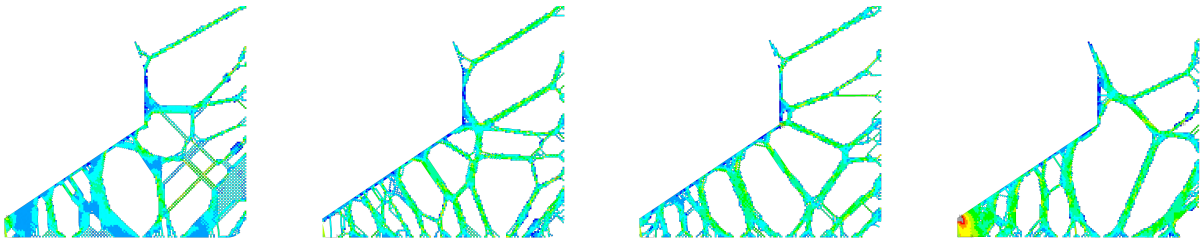

(a) (b) (c) (d)

Figure B.2: Web frame thickness of 15 [mm] (a) fully included start (b), (c) and (d) are random starts.

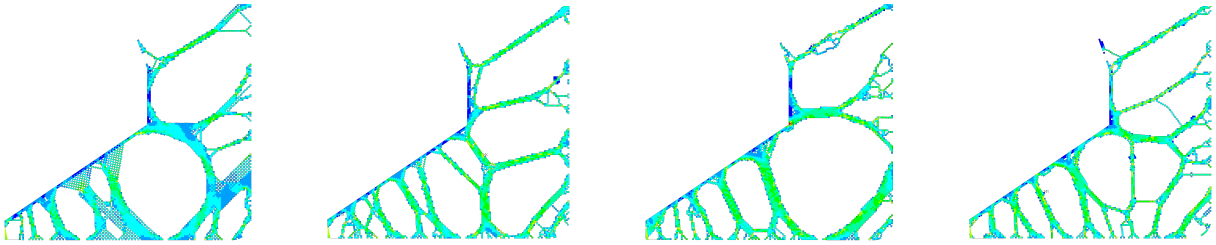

(a) (b) (c) (d)

Figure B.3: Web frame thickness of 18 [mm] (a) fully included start (b), (c) and (d) are random starts.

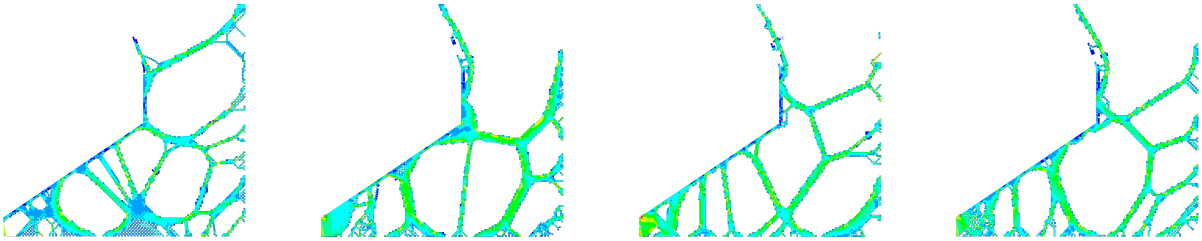

(a) (b) (c) (d)

Figure B.4: Web frame thickness of 21 [mm] (a) fully included start (b), (c) and (d) are random starts.

C
Supplementary Fundamental Model Results

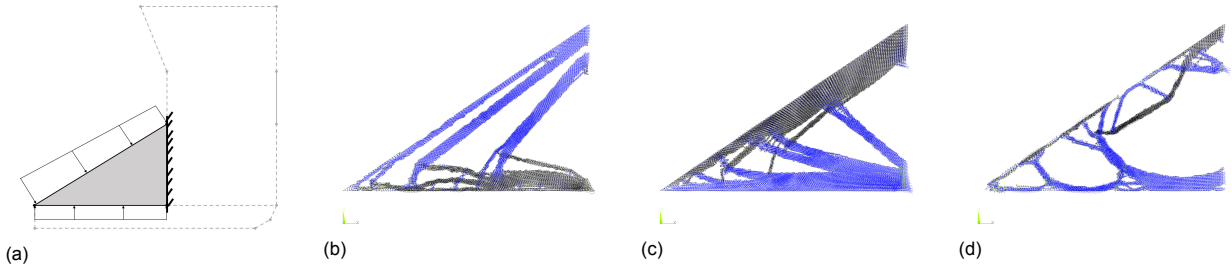

Figure C.1: Bottom of hopper tank fundamental model with (a) water pressure, (b) hopper pressure and (c) water and hopper pressure combined

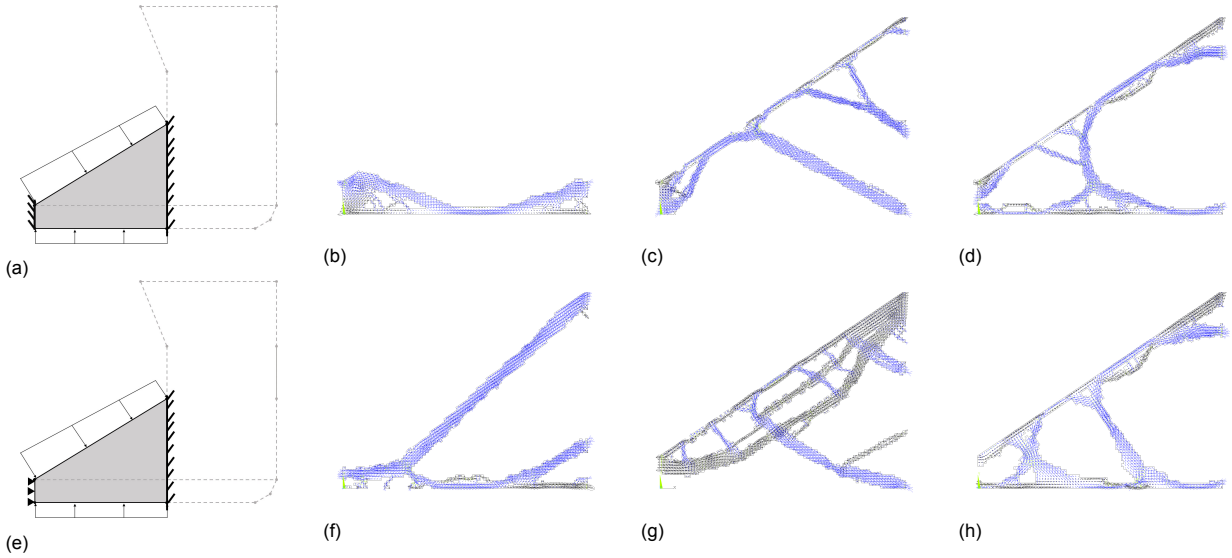

Figure C.2: Bottom of hopper tank with double bottom fundamental model with (a) water pressure, (b) hopper pressure and (c) water and hopper pressure combined

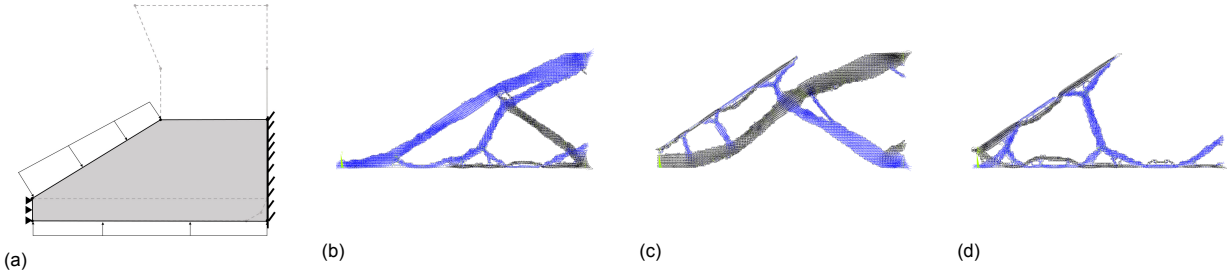

Figure C.3: Bottom of hopper tank with double bottom and side compartment fundamental model with (a) water pressure, (b) hopper pressure and (c) water and hopper pressure combined

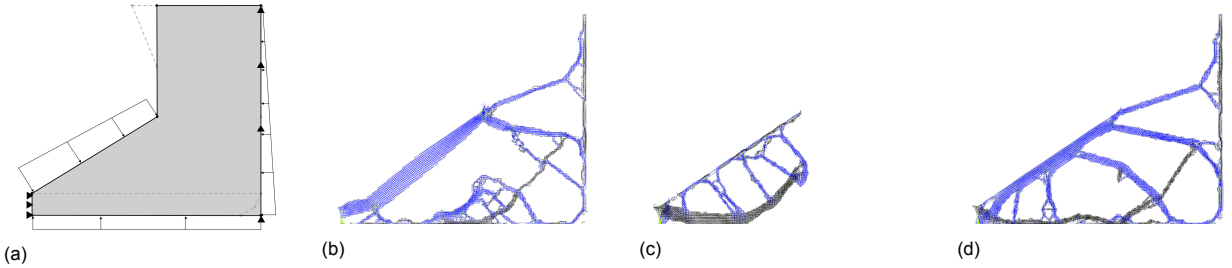

Figure C.4: Highly simplified TSHD midsection model with (a) water pressure, (b) hopper pressure and (c) water and hopper pressure combined

D

Supplementary Web Frame Topology Optimization Results

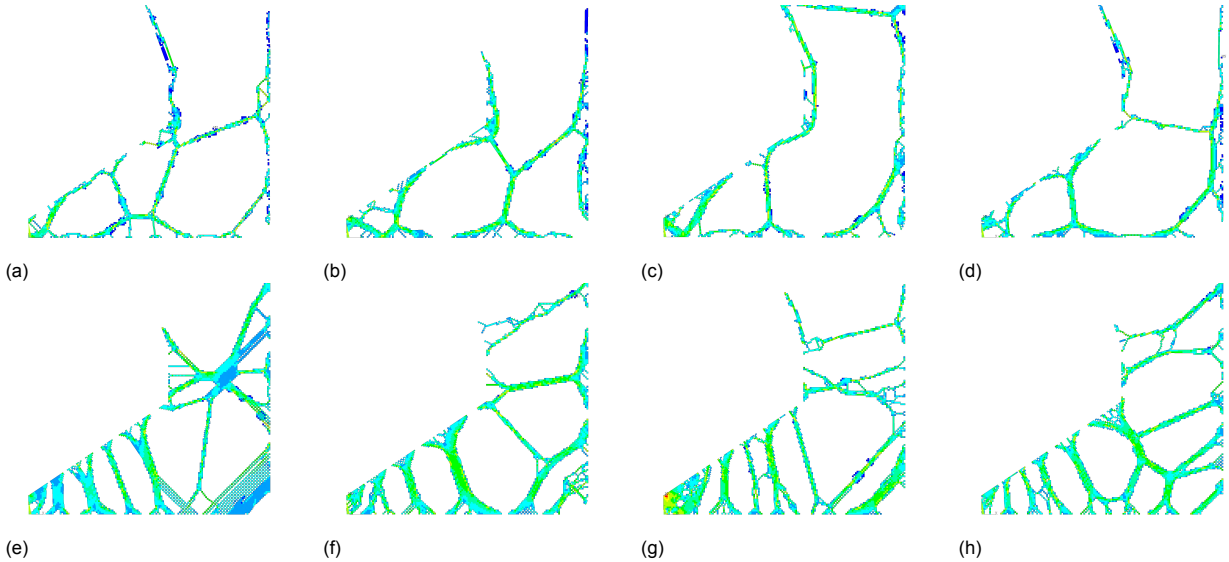

Figure D.1: **WFS of 562.5 [mm]**: (a) fully included start with web frame thickness of 18 [mm] (b), (c) and (d) are random starts with web frame thickness of 18 [mm]. (e) fully included start with web frame thickness of $18 \cdot \frac{1}{4}$ [mm] (f), (g) and (h) are random starts with web frame thickness of $18 \cdot \frac{1}{4}$ [mm]

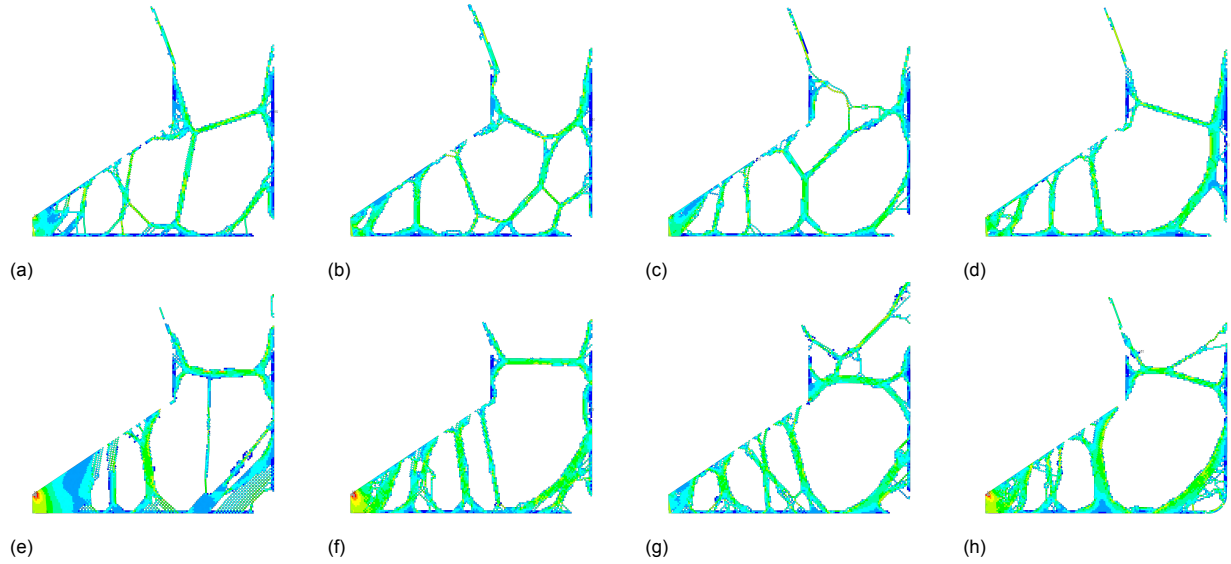

(a) (b) (c) (d)

(e) (f) (g) (h)

Figure D.2: **WFS of 1125 [mm]**: (a) fully included start with web frame thickness of 18 [mm] (b), (c) and (d) are random starts with web frame thickness of 18 [mm]. (e) fully included start with web frame thickness of $18 \cdot \frac{2}{4}$ [mm] (f), (g) and (h) are random starts with web frame thickness of $18 \cdot \frac{2}{4}$[mm]

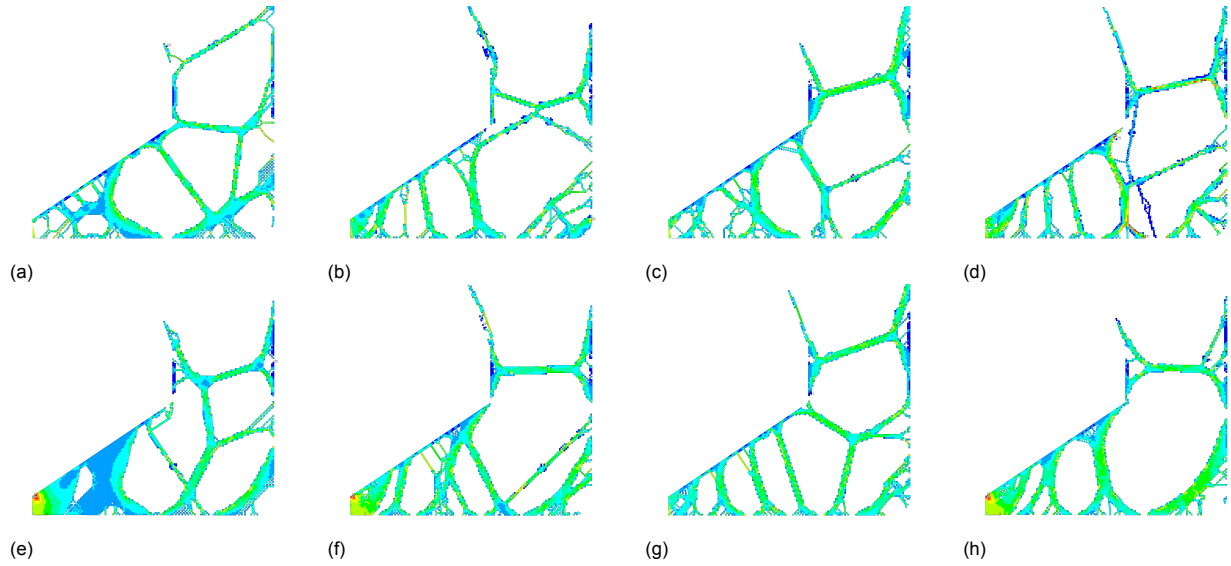

(a) (b) (c) (d)

(e) (f) (g) (h)

Figure D.3: **WFS of 1687.5 [mm]**: (a) fully included start with web frame thickness of 18 [mm] (b), (c) and (d) are random starts with web frame thickness of 18 [mm]. (e) fully included start with web frame thickness of $18 \cdot \frac{3}{4}$ [mm] (f), (g) and (h) are random starts with web frame thickness of $18 \cdot \frac{3}{4}$ [mm]

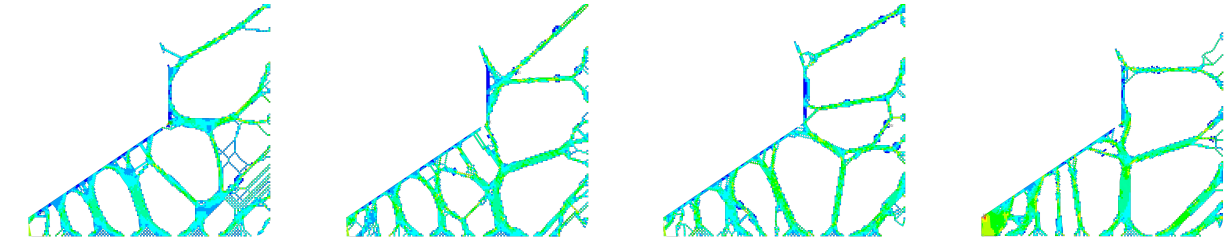

(a) (b) (c) (d)

Figure D.4: **WFS of 2250 [mm]**: (a) fully included start with web frame thickness of 18 [mm] (b), (c) and (d) are random starts with web frame thickness of 18 [mm].

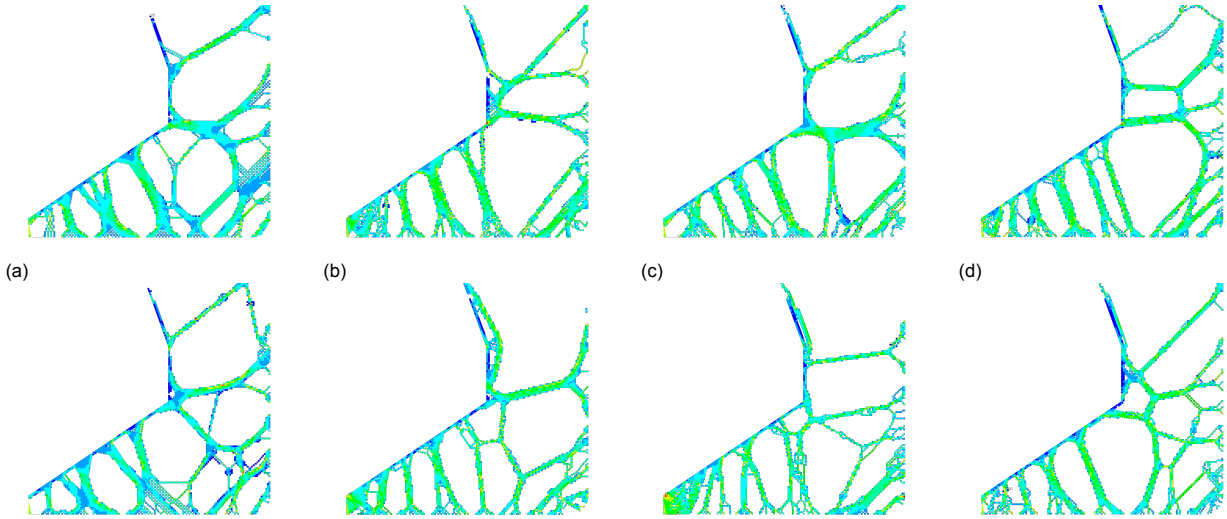

(a) (b) (c) (d)

(e) (f) (g) (h)

Figure D.5: **WFS of 2812.5 [mm]**: (a) fully included start with web frame thickness of 18 [mm] (b), (c) and (d) are random starts with web frame thickness of 18 [mm]. (e) fully included start with web frame thickness of $18 \cdot \frac{5}{4}$ [mm] (f), (g) and (h) are random starts with web frame thickness of $18 \cdot \frac{5}{4}$ [mm]

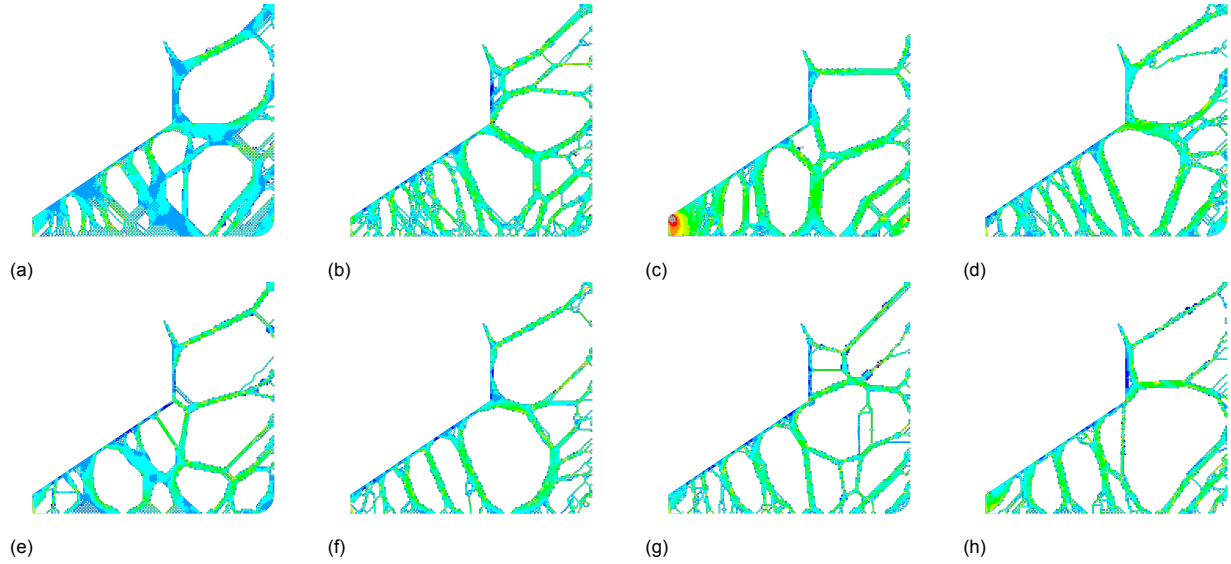

Figure D.6: **WFS of 3375 [mm]**: (a) fully included start with web frame thickness of 18 [mm] (b), (c) and (d) are random starts with web frame thickness of 18 [mm]. (e) fully included start with web frame thickness of $18 \cdot \frac{6}{4}$ [mm] (f), (g) and (h) are random starts with web frame thickness of $18 \cdot \frac{6}{4}$ [mm]

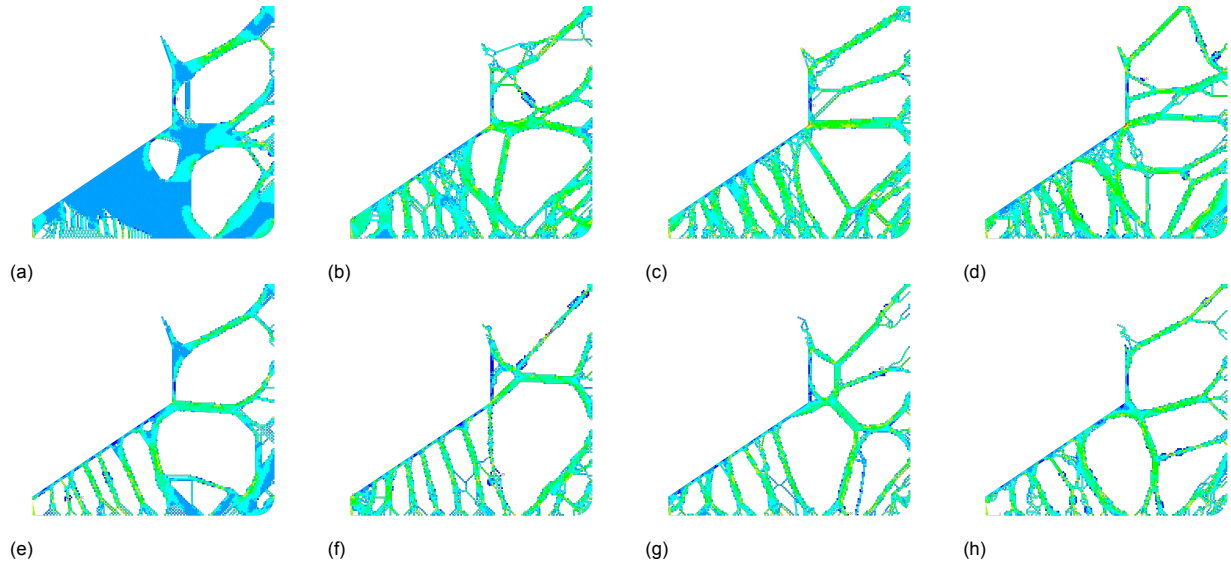

Figure D.7: **WFS of 3937.5 [mm]**: (a) fully included start with web frame thickness of 18 [mm] (b), (c) and (d) are random starts with web frame thickness of 18 [mm]. (e) fully included start with web frame thickness of $18 \cdot \frac{7}{4}$ [mm] (f), (g) and (h) are random starts with web frame thickness of $18 \cdot \frac{7}{4}$ [mm]

		025		050		075		100	125		150		175	
t_{wf} [mm]		18	4.5	18	9	18	13.5	18	18	22.5	18	27	18	31.5
n_e [-]	FI	2216	3648	4407	5542	4486	5904	5266	6739	6337	7698	5935	9666	6331
	BRS	2176	3075	4357	4985	4669	4906	4858	6222	5989	6616	5560	7507	5797
mass [t-]	FI	3.21	1.32	6.39	4.02	6.50	6.42	7.63	9.76	11.48	11.15	12.90	14.01	16.05
	BRS	3.15	1.11	6.31	3.61	6.77	5.33	7.04	9.02	10.85	9.59	12.08	10.88	14.70
$\sigma_{VM,max}$[MPa]	FI	177	165	296	469	177	468	220	163	194	165	168	182	178
	BRS	184	174	211	211	169	173	168	231	169	226	173	232	185

Table D.1: The number of elements, its mass and maximum Von Mises stress of the topology optimizations

Bibliography

[1] Grégoire Allaire, François Jouve, and Anca Maria Toader. A level-set method for shape optimization. *Comptes Rendus Mathematique*, 334(12):1125–1130, 2002. ISSN 1631073X. doi: 10.1016/S1631-073X(02)02412-3.

[2] ANSYS Inc. ANSYS Mechanical APDL Substructuring Analysis Guide. 3304(April):724–746, 2015.

[3] M. P. Bendsøe, N. Olhoff, and O. Sigmund. *IUTAM Symposiumon Topological DesignOptimization of Structures,Machines and MaterialsStatus and Perspectives*. 2005. ISBN 964-7445-88-1.

[4] Joshua D. Deaton and Ramana V. Grandhi. A survey of structural and multidisciplinary continuum topology optimization: Post 2000, jan 2014. ISSN 1615147X.

[5] Building Engineering and G P Steven. An evolutionary m e t h o d for optimal design of plates with discrete variable thicknesses subject to constant weight. (Ringertz 1988): 55–64, 2006.

[6] Y. Garbatov and P. Georgiev. Optimal design of stiffened plate subjected to combined stochastic loads. In *Progress in the Analysis and Design of Marine Structures - Proceedings of the 6th International Conference on Marine Structures, MARSTRUCT 2017*, pages 243–252, 2017. ISBN 9781138069077. doi: 10.1201/9781315157368-29.

[7] Jae Dong Kim, Beom Seon Jang, Tae Yoon Park, and Sangbae Jeon. FEA based optimization for stiffened plate considering buckling and yield strength. In *Progress in the Analysis and Design of Marine Structures - Proceedings of the 6th International Conference on Marine Structures, MARSTRUCT 2017*, pages 193–202. CRC Press, 2017. ISBN 9781138069077. doi: 10.1201/9781315157368-24.

[8] S. Kirkpatrick, C. D. Gelatt, and M. P. Vecchi. Optimization by simulated annealing. *Science*, 220(4598):671–680, 1983. ISSN 00368075. doi: 10.1126/science.220.4598.671.

[9] Langermann. Langermann 2D Function. URL `http://infinity77.net/global{_}optimization/{_}images/Langermann.png`.

[10] D Leidenfrost. the 46M Sailing Yacht Exo : Structural Design Inspired By Nature. (November), 2016.

[11] Martin Philip Bendsoe and Noboru Kikuchi. Generating optimal topologies in structural design using a homogenization method. *Computer Methods in Applied Mechanics and Engineering*, 71:197–224, 1988.

[12] A.G.M. Michell. LVIII. The limits of economy of material in frame-structures . *The London, Edinburgh, and Dublin Philosophical Magazine and Journal of Science*, 8(47): 589–597, 1904. ISSN 1941-5982. doi: 10.1080/14786440409463229.

[13] Chara Ch Mitropoulou, Yiannis Fourkiotis, Nikos D. Lagaros, and Matthew G. Karlaftis. *Evolution Strategies-Based Metaheuristics in Structural Design Optimization*, volume 2. Elsevier Inc., first edit edition, 2013. ISBN 9780123983640. doi: 10.1016/B978-0-12-398364-0.00004-8. URL `http://dx.doi.org/10.1016/B978-0-12-398364-0.00004-8`.

[14] Marcin Molga and Czesław Smutnicki. Test functions for optimization needs. (c):1–43, 2005.

[15] M A O Montes. Topology Optimization Algorithms for the Solution of Compliance and Volume Problems in 2D. Technical report, 2016.

[16] David J. Munk, Gareth A. Vio, and Grant P. Steven. Topology and shape optimization methods using evolutionary algorithms: a review. *Structural and Multidisciplinary Optimization*, 52(3):613–631, sep 2015. ISSN 16151488. doi: 10.1007/s00158-015-1261-9.

[17] Y Okumoto, Y Takeda, M Mano, and T Okada. *Design of Ship Hull Structures*. 2009. ISBN 9783540884446. doi: 10.1007/978-3-540-88445-3. URL https://link.springer.com/content/pdf/10.1007{%}2F978-3-540-88445-3.pdf.

[18] Jeom Kee Paik. Chapter 12: Elastic Buckling of Plates. In *Ship Structural Analysis and Design*. 2010.

[19] Jeom Kee Paik and Bong Ju Kim. Ultimate strength formulations for stiffened panels under combined axial load, in-plane bending and lateral pressure: A benchmark study. *Thin-Walled Structures*, 40(1):45–83, jan 2002. ISSN 02638231. doi: 10.1016/S0263-8231(01)00043-X.

[20] Jeom Kee Paik, Ge Wang, Bong Ju Kim, and Anil Kumar Thayamballi. *Ultimate limit state design of ship hulls*, volume 110. 2003.

[21] O. M. Querin, G. P. Steven, and Y. M. Xie. Evolutionary structural optimisation (ESO) using a bidirectional algorithm. *Engineering Computations (Swansea, Wales)*, 15(8):1031–1048, 1998. ISSN 02644401. doi: 10.1108/02644409810244129.

[22] Ralf Tschullik, Hannes Prommer, Pentscho Pentschew, and Patrick Kaeding. Design concepts of double bottom sections based on topology optimization. *11th International Symposium on Practical Design of Ships and Other Floating Structures, PRADS 2010*, 1: 516–522, 2010.

[23] R. Bronsart W. Fricke. *Proceedings of the 20 Th International Ship and Offshore Structures Congress*, volume One. 2012. ISBN 0080436021. URL http://139.30.101.246/ISSC2012/images/stories/Proceedings/issc2012-vol1.pdf.

[24] Liang Xia, Qi Xia, Xiaodong Huang, and Yi Min Xie. Bi-directional Evolutionary Structural Optimization on Advanced Structures and Materials: A Comprehensive Review. *Archives of Computational Methods in Engineering*, 25(2):437–478, apr 2018. ISSN 18861784. doi: 10.1007/s11831-016-9203-2.

[25] Y.M. Xie and G.P. Steven. Technical Note a Simple Approach To Structural Optimization. *Compurers & Structures*, 49(5):885–896, 1993.